GLIA

WILEY

ORIGINAL RESEARCH ARTICLE

Gray and white matter astrocytes differ in basal metabolism but respond similarly to neuronal activity

Susanne Köhler[1] | Ulrike Winkler[1] | Tabea Junge[1] | Kristina Lippmann[1] | Jens Eilers[1] | Johannes Hirrlinger[1,2]

[1]Faculty of Medicine, Carl-Ludwig-Institute for Physiology, Leipzig University, Leipzig, Germany

[2]Department of Neurogenetics, Max-Planck-Institute for Multidisciplinary Sciences, Göttingen, Germany

Correspondence
Johannes Hirrlinger, Faculty of Medicine, Carl-Ludwig-Institute for Physiology, Leipzig University, Liebigstr. 27, D-04103 Leipzig, Germany.
Email: johannes.hirrlinger@medizin.uni-leipzig.de and hirrlinger@mpinat.mpg.de

Abstract

Astrocytes are a heterogeneous population of glial cells in the brain, which adapt their properties to the requirements of the local environment. Two major groups of astrocytes are protoplasmic astrocytes residing in gray matter as well as fibrous astrocytes of white matter. Here, we compared the energy metabolism of astrocytes in the cortex and corpus callosum as representative gray matter and white matter regions, in acute brain slices taking advantage of genetically encoded fluorescent nanosensors for the $NADH/NAD^+$ redox ratio and for ATP. Astrocytes of the corpus callosum presented a more reduced basal $NADH/NAD^+$ redox ratio, and a lower cytosolic concentration of ATP compared to cortical astrocytes. In cortical astrocytes, the neurotransmitter glutamate and increased extracellular concentrations of K^+, typical correlates of neuronal activity, induced a more reduced $NADH/NAD^+$ redox ratio. While application of glutamate decreased [ATP], K^+ as well as the combination of glutamate and K^+ resulted in an increase of ATP levels. Strikingly, a very similar regulation of metabolism by K^+ and glutamate was observed in astrocytes in the corpus callosum. Finally, strong intrinsic neuronal activity provoked by application of bicuculline and withdrawal of Mg^{2+} caused a shift of the $NADH/NAD^+$ redox ratio to a more reduced state as well as a slight reduction of [ATP] in gray and white matter astrocytes. In summary, the metabolism of astrocytes in cortex and corpus callosum shows distinct basal properties, but qualitatively similar responses to neuronal activity, probably reflecting the different environment and requirements of these brain regions.

KEYWORDS
astrocyte, energy metabolism, gray matter, heterogeneity, white matter

1 | INTRODUCTION

Astrocytes are a heterogeneous type of glial cells in the brain, which have been classified in several different subpopulations. These include

---

protoplasmic astrocytes residing in gray matter (GM), and fibrous astrocytes localized within white matter (WM) (Köhler et al., 2021; Matyash & Kettenmann, 2010; Miller & Raff, 1984; Schitine et al., 2015; Sofroniew & Vinters, 2010). These two populations of astrocytes differ substantially in their morphology: protoplasmic astrocytes are characterized by round somata and highly branched processes, while the cell bodies of fibrous astrocytes are more elongated and processes are long, thin and less-branched running parallel to neuronal axons in WM. Many other properties are also different, like their development during gliogenesis (Bribián et al., 2016; García-Marqués & López-Mascaraque, 2013; Luskin & McDermott, 1994), their mRNA and protein expression levels (Aberg & Kozlova, 2000; Bachoo et al., 2004; Bignami et al., 1972; Yeh et al., 2009) as well as their susceptibility to ischemia (Hamner et al., 2011; Köhler et al., 2021; Matute et al., 2013; Pantoni et al., 1996; Shannon et al., 2007; Tekkok & Ransom, 2004; Wu et al., 2015). However, whether these different properties and the different metabolic demands in GM and WM are reflected by heterogeneity of energy metabolism of astrocytes has not been elucidated in detail so far (Köhler et al., 2021; Oberheim et al., 2012).

Astrocytes in GM are in close structural contact to neurons. They enwrap neuronal synapses with their fine processes forming "tripartite synapses," receive neuronal information and signal back to neurons by releasing gliotransmitters (Araque et al., 1999; Parpura & Zorec, 2010). Glutamate released at glutamatergic synapses is metabolized to glutamine in astrocytes and shuttled back to neurons within the glutamate-glutamine-cycle (Bak et al., 2006; Benjamin & Quastel, 1974; Norenberg & Martinez-Hernandez, 1979; Tani et al., 2014). Astrocytes supply neurons with energy substrates, and contribute to neurotransmitter metabolism and ion homeostasis (Allaman et al., 2011; Araque et al., 1999; Bak et al., 2006; Bolaños, 2016; Díaz-García et al., 2017; DiNuzzo et al., 2012; Farhy-Tselnicker & Allen, 2018; Hertz & Zielke, 2004; Newman, 1986; Pellerin & Magistretti, 1994, 2012; Sofroniew & Vinters, 2010; Walz, 2000). For example, glutamate and potassium (K^+) released from active neurons are taken up by astrocytes and stimulate astrocytic metabolism, including glycolysis and lactate release (Bittner et al., 2011; Choi et al., 2012; Fernandez-Moncada et al., 2018; Köhler et al., 2018; MacVicar & Choi, 2017; Pellerin & Magistretti, 1994; Ruminot et al., 2017; Sotelo-Hitschfeld et al., 2012; Xu et al., 2013). The concentration of cytosolic ATP ([ATP]) decreases when GM astrocytes are exposed to glutamate, while it increases in response to a higher extracellular concentration of K^+ ($[K^+]_e$) (Fernandez-Moncada et al., 2018; Lerchundi et al., 2019, 2020; Magistretti & Chatton, 2005; Winkler et al., 2017). In awake mice, arousal induced neuronal activity in the cortex stimulates glycolytic activation and lactate release from astrocytes (Zuend et al., 2020). In summary, the energy metabolism of protoplasmic astrocytes in GM is closely associated with neuronal activity and signal processing.

Fibrous astrocytes in WM face a different situation, most likely coinciding with different metabolic requirements. Neuronal axons in WM propagate action potentials, but there is much less if any neuronal information processing taking place. Nevertheless, glutamate and

K^+ are also released from WM axons (Kukley et al., 2007; Wake et al., 2011; Ziskin et al., 2007). In many cases, axons are myelinated and astrocytes only have direct contact to axons at the node of Ranvier. Therefore, also oligodendrocytes contribute to energy metabolism in WM (Fünfschilling et al., 2012; Hirrlinger & Nave, 2014; Lee et al., 2012; Nave, 2010b; Saab et al., 2016; Trevisiol et al., 2020). Action potential propagation and axonal function depends on astrocytic glycogen as an energy fuel (Brown et al., 2005; Fern et al., 1998; Tekkok et al., 2005; Waitt et al., 2017; Wender et al., 2000), and inhibiting lactate transporters in the optic nerve impairs axonal ATP maintenance during electrical activity (Trevisiol et al., 2017). However, evidence from the corpus callosum suggests that glucose rather than lactate is transferred between glial cells and neurons (Meyer et al., 2018). Taken together, the detailed mechanisms of metabolite transfer as well as the regulation of energy metabolism in fibrous astrocytes according to neuronal energy demand remain to be elucidated.

In this study, we took advantage of genetically encoded fluorescent nanosensors (Hirrlinger & Nimmerjahn, 2022; Koveal et al., 2020; San Martín et al., 2022; San Martín, Sotelo-Hitschfeld, et al., 2014) reporting the NADH/NAD$^+$ redox state (Peredox-mCherry; Hung et al., 2011) or the cytosolic concentration of ATP (ATeam1.03YEMK; Imamura et al., 2009) to investigate the dynamics of energy metabolism of astrocytes in cortex (i.e., GM) and corpus callosum (i.e., WM) in acute brain slices. Different imaging techniques revealed a more reduced NADH/NAD$^+$ redox state and lower ATP levels in WM astrocytes. Exposing astrocytes to glutamate, increased concentrations of extracellular K^+ or intense neuronal activity disclosed qualitatively similar responses of energy metabolism in GM and WM astrocytes.

2 | MATERIAL AND METHODS

2.1 | Ethics statement

All experiments were performed in accordance with the guidelines for the welfare of experimental animals issued by the European Communities Council Directive (2010/63/EU) and with the German Protection of Animals Act (Tierschutzgesetz). C57/Bl6 mice were bred in the animal facility of the Medical Faculty of Leipzig University and were housed in individually ventilated cages in a specific pathogen free environment in a 12/12 h light dark cycle with access to food and water ad libitum. Experiments were approved by the animal welfare office of the University Medical Center, Leipzig, as well as the local governmental authorities (Landesdirektion Leipzig, registration numbers T04/13, T20/16, and TVV62/15).

2.2 | Peredox and ATeam imaging in astrocytes in acutely isolated brain slices

To image the dynamics of the NADH/NAD$^+$ redox state as well as of the ATP concentration in astrocytes in the cortex (Ctx) and

corpus callosum (CC) in acute brain slices, the open reading frames of Peredox (Peredox-mCherry, Hung et al., 2011) or ATeam (ATeam1.03YEMK, Imamura et al., 2009) were cloned into vectors for adeno-associated virus (AAV) mediated expression. Astrocyte-specific expression was achieved by GFAP-promoter elements (Lee et al., 2008; Mächler et al., 2016; Stobart et al., 2018) as described recently for ATeam (Köhler et al., 2020). AAVs (serotype 5) were obtained from the Viral Vector Facility at the Neuroscience Center Zurich, University of Zurich, Switzerland. About 0.5 μl of AAV containing solution (virus titer: Peredox: 1.8×10^{12} vg/ml; ATeam: 2.75×10^{12} vg/ml) were injected stereotactically into the brain of 2- to 3-month old mice using the following coordinates relative to bregma: Ctx: - 0.5 mm caudal, lateral 2.0 mm, ventral 1.1 mm; CC: - 1.9 mm caudal, lateral 0.2 mm, ventral 1.4 mm. Four weeks after injection, mice were sacrificed and 250 μm thick coronal brain slices were prepared as described previously (Köhler et al., 2020; Pätz et al., 2018). Imaging experiments were performed with a 2-photon laser scanning microscope (Olympus FV1000, Olympus, Tokyo, Japan) equipped with a XLPlan N 25x/1.05 W objective (Olympus) and a Mai Tai DeepSee laser (Spectra-Physics, Darmstadt, Germany) with the following imaging parameters for Peredox (wavelengths): excitation: 800 nm; beamsplitter 570 nm; emission (T-Sapphire): BP495-540 nm; emission (mCherry): BP575-630 nm. For ATeam: excitation: 810 nm, beamsplitter 510 nm; emission (CFP): BP460-500 nm. Pixel size: 0.552×0.552 μm; 512×512 pixels; pixel dwell time: 2 μs; time resolution: 60 s; stack of 23 z-planes. Acute slices were continuously perfused at room temperature with artificial cerebrospinal fluid (aCSF, in mM: 130 NaCl, 2.5 KCl, 1 $MgCl_2$, 2 $CaCl_2$, 1.25 NaH_2PO_4, 26 $NaHCO_3$, 10 Glucose, pH 7.4) and bubbled with carbogen (95% O_2, 5% CO_2). Glucose was omitted in solutions containing lactate and pyruvate. All solutions were adjusted to the same pH and osmolality. The following drugs and concentrations were used: lactate (10 mM, Applichem, Darmstadt, Germany); pyruvate (10 mM, Sigma-Aldrich, St. Louis, USA); glutamate (100 μM, AppliChem); bicuculline methiodide (10 μM, Sigma-Aldrich); tetrodotoxin (TTX, 1 μM, Tocris, Bristol, UK); sodium azide (10 mM, Serva, Heidelberg, Germany); sodium iodoacetate (1 mM, Sigma-Aldrich). ACSF with higher potassium concentrations of 5 or 10 mM will be referred to as K5 or K10, respectively.

At the beginning of each experiment, slices were transferred to a submerged recording chamber and superfused with control aCSF for 20 min to establish the baseline sensor signal. Thereafter, different substances/neurotransmitter solved in aCSF were bath-applied for 10–20 min for each condition. About 10 mM lactate and 10 mM pyruvate were applied consecutively at the end of experiments with Peredox to establish the dynamic range of the sensor as described previously (Hung et al., 2011; Köhler et al., 2018; Mongeon et al., 2016), before azide (10 mM) +iodoacetate (1 mM) was finally applied (Figure S1). Solutions containing neurotransmitters or an increased K^+ concentration were supplemented with tetrodotoxin (TTX; 1 μM). TTX prevents action potential firing allowing to study action potential-

independent effects of these treatments on astrocytes. For experiments with bicuculline, no Mg^{2+} was added to the aCSF to avoid a Mg^{2+} block of NMDA receptors.

The mean gray scale value within a manually defined region of interest (ROI) containing a single cell was calculated for each imaging channel using Fiji (Schindelin et al., 2012). The Peredox signal was calculated as the ratio of the intensity of the T-Sapphire channel and the intensity of the mCherry channel (Hung & Yellen, 2014; Köhler et al., 2018), while the ATeam signal was calculated as the FRET/CFP ratio (Köhler et al., 2020; Trevisiol et al., 2017). Data was corrected for baseline drift. For Peredox, the sensor signal was converted into the NADH/NAD$^+$ redox ratio using the calibration described below. For ATeam a similar calibration could not be performed due to the difficulties to modulate intracellular ATP concentrations in a quantitative manner for calibration as well as to obtain reliable R_{min} and R_{max} values within each experiment. Therefore, data on the NADH/NAD$^+$ redox state is given as NADH/NAD$^+$ redox ratio, while data on ATP is presented as ATeam sensor signal. Treatment effects are shown as the difference of data averaged for the last 2–5 min of treatment and the last 5 min of pre-incubation in aCSF prior to treatment (ΔNADH/NAD$^+$; ΔATeam signal).

2.3 | Fluorescence lifetime imaging (FLIM)

Brain slices were prepared as described above. The slices were constantly superfused with carbogen-bubbled aCSF and live-FLIM of Peredox was performed using a 2-photon laser scanning microscope (Olympus BX50WI) equipped with a Spectra Physics Tsunami pulsed (80 MHz) laser, a 60× water-immersion objective (Olympus LumPlan 60×/0.9) and a FLIM system (TimeHarp 200, PicoQuant, Berlin, Germany). T-Sapphire of Peredox was excited at 800 nm and emitted fluorescence was detected through three consecutive emission filters SP610, SP625, and SP540 with a pixel size of 512×512. Data was analyzed using the software SymPhoTime64 (PicoQuant) and IgorPro8 (WaveMetrics Inc., Portland, USA).

For individual fluorescence decay curves, a semi-quantitative "empirical" lifetime was computed similar to the approach in Mongeon et al. (2016). In brief, the median photon arrival time from all photons detected within a time window of 6 ns after the steepest rise on the fluorescence lifetime was calculated; the exact form of the instrument function was not taken into consideration. In contrast to multi-exponential fitting approaches, the empirical lifetime is significantly less prone to errors induced by low signal-to-noise data, possible changes of the instrument response function at different positions of the field-of-view, and the uncertainties inherent to fitting noisy fluorescence data with multi-exponential fits (Li et al., 2020). Note that the time window of 6 ns of our analysis results in shorter empirical lifetimes than the time window of 10 ns used by Mongeon et al. (2016).

TABLE 1 Number of animals (*N*) and number of analyzed cells (*n*)

Figure	Condition	N (number of animals)		n (number of analyzed cells)	
		Cortex	Corpus callosum	Cortex	Corpus callosum
2a	Calibration				
	Lactate	7	5	114	98
	L/P = 50	5	4	62	34
	L/P = 20	5	4	87	40
	Pyruvate	7	5	121	102
2b/c/d	Baseline				
	FLIM (Lifetime)	7	5	120	96
	FLIM (NADH/NAD$^+$)	7	5	119	85
	Fl.ratio (NADH/NAD$^+$)	24	22	302	168
3d	Peredox				
	Glutamate	5	4	45	11
	[K$^+$]$_e$ = 5 mM	5	4	40	14
	[K$^+$]$_e$ = 10 mM	5	3	41	13
	Glutamate + [K$^+$]$_e$ = 5 mM	4	3	35	10
4a	ATeam				
	Baseline	19	14	343	237
4c	ATeam				
	Baseline	11	5	37	21
	azide + IA	11	5	37	21
4d/e	ATeam				
	Glutamate	6	6	92	83
	[K$^+$]$_e$ = 5 mM	4	5	102	52
	[K$^+$]$_e$ = 10 mM	4	5	102	52
	Glutamate + [K$^+$]$_e$ = 5 mM	5	5	80	30
5b	Field potential recordings	3	3	7 (slices)	7 (slices)
5c/d	Bicuculline				
	Peredox	4	4	48	29
	ATeam	4	5	69	72
S2A	Peredox-Baseline				
	+TTX	18	13	209	51
	−TTX	24	22	302	168
S2B	ATeam-Baseline				
	+TTX	15	9	274	165
	−TTX	19	14	343	237

2.4 | Calibration of the Peredox sensor

To calibrate the signal of Peredox to the NADH/NAD$^+$ redox ratio, lactate and pyruvate were applied to the slices in different concentration ratios. Lactate and pyruvate are taken up into astrocytes by monocarboxylate transporters and equilibrate with the NADH/NAD$^+$ redox ratio by the reaction of lactate dehydrogenase (LDH). To obtain the most oxidized (reflecting R_{min}) and most reduced (reflecting R_{max}) state, slices were superfused with pyruvate (10 mM) and lactate (10 mM), respectively. In addition, slices were superfused with aCSF

containing lactate and pyruvate in concentration ratios [lactate]/[pyruvate] (L/P) of 50 and 20 at [lactate] = 10 mM, corresponding to a NADH/NAD$^+$ redox ratio of 0.014 and 0.0056, respectively, given the thermodynamic equilibration constant of the LDH reaction $k = 1.1 \times 10^{-11}$ M and assuming a cytosolic pH of 7.4 (Hung & Yellen, 2014; Köhler et al., 2018). To obtain a calibration function, the data was fitted using a sigmoidal equation $f_{sensor} = R_{min} + \Delta R_{max} * x/(k_D + x)$; with f_{sensor}: sensor signal (Peredox fluorescence lifetime or T-Sapphire/mCherry fluorescence ratio) and x: NADH/NAD$^+$ redox ratio (Sigmaplot 12.0; Systat, Erkrath, Germany). This calibration was

performed for both fluorescence lifetime imaging (FLIM) and ratiometric 2-photon fluorescence intensity imaging and the calibration curves were used to calculate the NADH/NAD$^+$ redox ratio from the Peredox signal in further experiments.

2.5 | Field potential recordings

For local field potential (LFP) recordings, acute brain slices were prepared as described above and stored under submerged conditions at room temperature. Recording electrodes were pulled from filamented borosilicate glass (Hilgenberg, Germany) with a resistance of around 4–6 MΩ when filled with aCSF. Electrodes were placed both in Ctx (L3) and CC (above the hippocampal area CA1), that is, the same areas as used for imaging experiments. LFP recordings were conducted under submerged conditions, signals were pre-amplified (100×, EXT-10C), filtered at 3 kHz (LPBF-01GX) and once more amplified (10×, PA-2S, all instruments from npi electronic GmbH, Tamm, Germany). Signals were digitized (Micro1401-3, CED, Cambridge, UK) and stored for off-line analysis using Spike2v9.01 (CED, Cambridge, UK). Offline, data underwent a DC removal (time constant of 0.5 s) and were low pass-filtered (25 Hz). Single events were manually analyzed using Spike2.

2.6 | Immunohistochemical analysis

Mice were transcardially perfused with 4% paraformaldehyde in phosphate buffered saline (PBS: 137 mM NaCl, 2.7 mM KCl, 8 mM Na$_2$HPO$_4$, 0.15 mM KH$_2$PO$_4$, pH 7.4). The brain was removed from the scull and post-fixed for 24 h in the same fixative. About 45 μm thick vibratome sections were prepared and stained for the pan-astrocyte marker 3-phosphoglycerate dehydrogenase (3PGDH; Yamasaki et al., 2001) using a guinea pig anti-3PGDH antibody (1:200, Frontier Institute, Ishikari, Hokkaido, Japan) and a donkey anti guinea pig CF633 (1:250, Sigma-Aldrich) in combination with a goat anti-GFP (Biotin conjugated) antibody (1:200, Rockland Immunochemicals, Pottstown, PA) and Streptavidin-Cy2 (1:500, Dianova, Hamburg, Germany). The staining protocol was previously described in detail (Winkler et al., 2013). Sections were mounted in ImmunoSelect Anti-fading Mounting Medium DAPI (Dianova). Images were acquired using a confocal laser scanning microscope (Olympus IX-71) equipped with an Olympus UApo/340 40×/1.35 oil immersion objective (Olympus, Hamburg, Germany).

2.7 | Statistics and data presentation

All experiments were performed on cells of at least three independently prepared brain slices from different mice. N (numbers of different mice used) and n (numbers of cells analyzed) are given in Table 1. Summarized data are shown as boxplots with the box spanning from 25th to 75th percentile, the whiskers spanning from 5th to the 95th percentile. Next to each boxplot, the same data set is presented as a dot plot showing all individual data points. The plus sign within the box represents the mean value, solid lines show the median. Gray boxplots represent data from cortical astrocytes (i.e., gray matter astrocytes), while white boxplots show data from astrocytes within the corpus callosum (i.e., white matter astrocytes). To illustrate treatment effects, the baseline prior to application of the treatment was subtracted to show change of the NADH/NAD$^+$ redox state (ΔNADH/NAD$^+$ = NADH/NAD^+_t − NADH/NAD$^+_{baseline}$; with NADH/NAD^+_t representing the NADH/NAD$^+$ at a timepoint of interest t) or the change of the ATeam sensor signal (ΔATeam signal = ATeam signal$_t$ − ATeam signal$_{baseline}$). Time resolved traces show the sliding average of three time points. GraphPad Prism was used for statistical analysis and data presentation. Final figures were arranged using Corel Draw. Statistical analysis of comparisons to baseline conditions (paired data) was done by Wilcoxon Signed Rank Test and asterisks (*) indicate significant differences compared to baseline. Data of Ctx and CC was compared by nested *t*-test (Figures 2b–d, 4a,c, and 5c) or nested ANOVA followed by Holm-Šídák post-hoc test (Figures 2a and 3d; Figure S2A,B), taking the different mice from which slices were prepared as subgroup classifier. Electrophysiological data was compared by Kruskal-Wallis One Way Analysis of Variance on Ranks (Figure 5b). # indicates significant differences compared to specific conditions as indicated in the figures. $p < .05$ was considered as statistically significant.

3 | RESULTS

To study the dynamics of energy metabolites in protoplasmic and fibrous astrocytes genetically encoded fluorescent sensors for the cytosolic NADH/NAD$^+$ redox state (Peredox; Hung et al., 2011) and the cytosolic concentration of ATP (ATeam1.03YEMK; abbreviated as "ATeam" in the following; Imamura et al., 2009) were expressed in astrocytes in situ by AAV-mediated gene transfer driven by the GFAP-promoter and stereotactic injections into cortex (Ctx) and corpus callosum (CC). Cells expressing the sensors showed the typical morphology of gray matter protoplasmic astrocytes and white matter fibrous astrocytes, respectively (Figure 1), reflecting their well described morphological differences (Oberheim et al., 2012; Somjen, 1988; Wang & Bordey, 2008). Indeed, most cells expressing the sensor stained for the pan-astrocyte marker 3-phoshoglycerate-dehydrogenase (Yamasaki et al., 2001, Ctx: 97% of 396 cells analyzed from 3 mice; CC: 92% of 188 cells from 2 mice), indicating that the vast majority of cells analyzed in the following were astrocytes.

The NADH/NAD$^+$ redox state was studied in both astrocytic subpopulations taking advantage of the sensor Peredox (Hung et al., 2011), and analyzed using fluorescence lifetime microscopy (FLIM; Mongeon et al., 2016). To calibrate the fluorescence lifetime of Peredox to the NADH/NAD$^+$ redox ratio, lactate and pyruvate were applied to the slices in different concentration ratios (Figure 2a). These treatments shift the cytosolic NADH/NAD$^+$ redox ratio, as
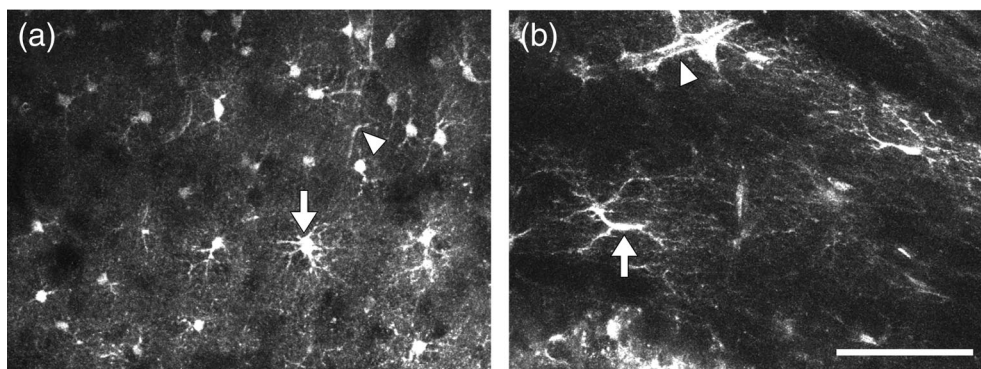
FIGURE 1 Morphology of astrocytes expressing fluorescent nanosensors in gray and white matter. Protoplasmic astrocytes in cortex (a; gray matter) and fibrous astrocytes in the corpus callosum (b; white matter) expressing the Peredox sensor imaged with 2-photon-microscopy. The T-Sapphire channel of Peredox is shown. Note the large somata of protoplasmic astrocytes (arrow in a) with their highly branched processes as well as the elongated cell bodies of fibrous astrocytes (arrow in b) with their long processes orientated parallel to neuronal axons. Arrowheads highlight astrocytic endfeet contacting blood vessels. Scale bar: 50 μm

both lactate and pyruvate are readily taken up into astrocytes by monocarboxylate transporters (MCTs; Pierre & Pellerin, 2005) and equilibrate with the NADH/NAD$^+$ redox ratio due to the high activity of lactate dehydrogenase (LDH) in astrocytes (Hung et al., 2011; Köhler et al., 2018). Application of lactate, pyruvate or both compounds in different concentration ratios resulted in the expected step-wise change in fluorescence lifetime of Peredox in astrocytes in both Ctx and CC (Figure 2a), ranging from 1.28 to 1.02 ns (median Ctx) and 1.34 to 1.04 ns (median CC) for lactate and pyruvate, respectively, which corresponds to a proportional change of 1.26 and 1.29. These data indicate that the fluorescence lifetime of Peredox is a sensitive readout for the NADH/NAD$^+$ redox ratio.

A longer fluorescence lifetime was observed in astrocytes of the CC compared to cortical astrocytes under baseline conditions (aCSF with 10 mM glucose), indicating a more reduced basal NADH/NAD$^+$ redox state (Figure 2b). Using the calibration (Figure 2a; see methods for details), the corresponding NADH/NAD$^+$ redox ratio values were calculated, which were significantly higher in astrocytes in the CC compared to cortical astrocytes (Figure 2c). By analyzing the Peredox sensor signal using the ratio of the fluorescence intensity of its two fluorophores (T-Sapphire/mCherry) instead of FLIM the same result was obtained for the NADH/NAD$^+$ redox ratio (Figure 2d; data of both Ctx and CC is not significantly different compared to the data obtained by FLIM for Ctx and CC, respectively, as shown in Figure 2c). Of note, the analysis of Peredox fluorescence both using ratiometric intensity and fluorescence lifetime measurements showed a rather broad distribution under baseline conditions, a finding which is well in line with the previously reported substantial variability of the NADH/NAD$^+$ redox state in astrocytes (Hung et al., 2011; Köhler et al., 2018; Mongeon et al., 2016). Taken together, white matter astrocytes in the CC have a more reduced cytosolic NADH/NAD$^+$ redox state than gray matter astrocytes in Ctx indicating heterogeneity of the energy metabolism of these two astrocytic cell populations in unstimulated conditions.
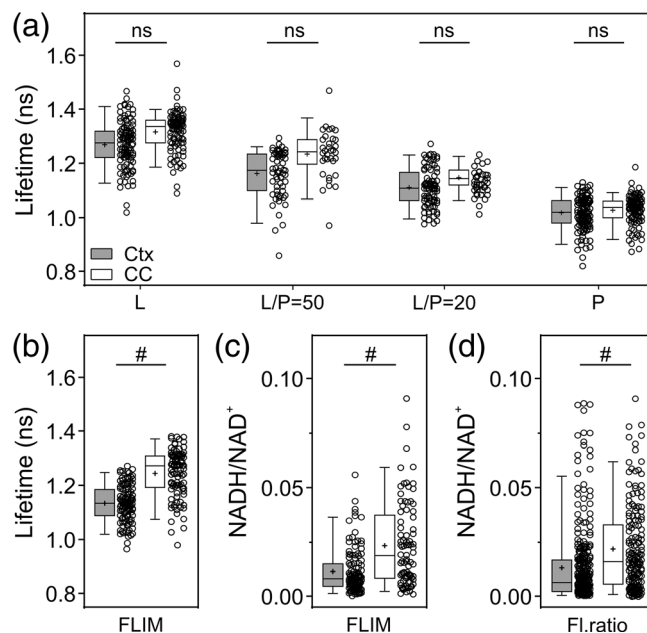
FIGURE 2 Characterization of the basal cytosolic NADH/NAD$^+$ redox state in astrocytes in the cortex and corpus callosum in acute brain slices. (a) The fluorescence lifetime of the Peredox sensor in astrocytes in acute brain slices, measured by FLIM, depends on the concentration ratios of lactate and pyruvate (L/P = [lactate]/[pyruvate]). L, P: application of lactate (10 mM) or pyruvate (10 mM), respectively, in the absence of the other compound. (b) Fluorescence lifetime of Peredox in astrocytes in Ctx (gray box) and CC (white box) under baseline conditions (aCSF with 10 mM glucose). (c) The NADH/NAD$^+$ redox ratio under baseline conditions is more reduced in astrocytes in the CC compared to Ctx. The NADH/NAD$^+$ redox ratio was calculated from the fluorescence lifetime data shown in (b) using the calibration data shown in (a). (d) The NADH/NAD$^+$ redox ratio in astrocytes in Ctx and CC under baseline conditions quantified using ratiometric 2-photon fluorescence intensity imaging confirms the more reduced NADH/NAD$^+$ redox state in astrocytes in CC compared to Ctx. Significant differences between the conditions are indicated ($^\#p$ < .05; ns: no significant difference, p > .05). For number of cells (n) and animals (N) see Table 1. Next to each boxplot, the same data set is presented as a dot plot showing all individual data points
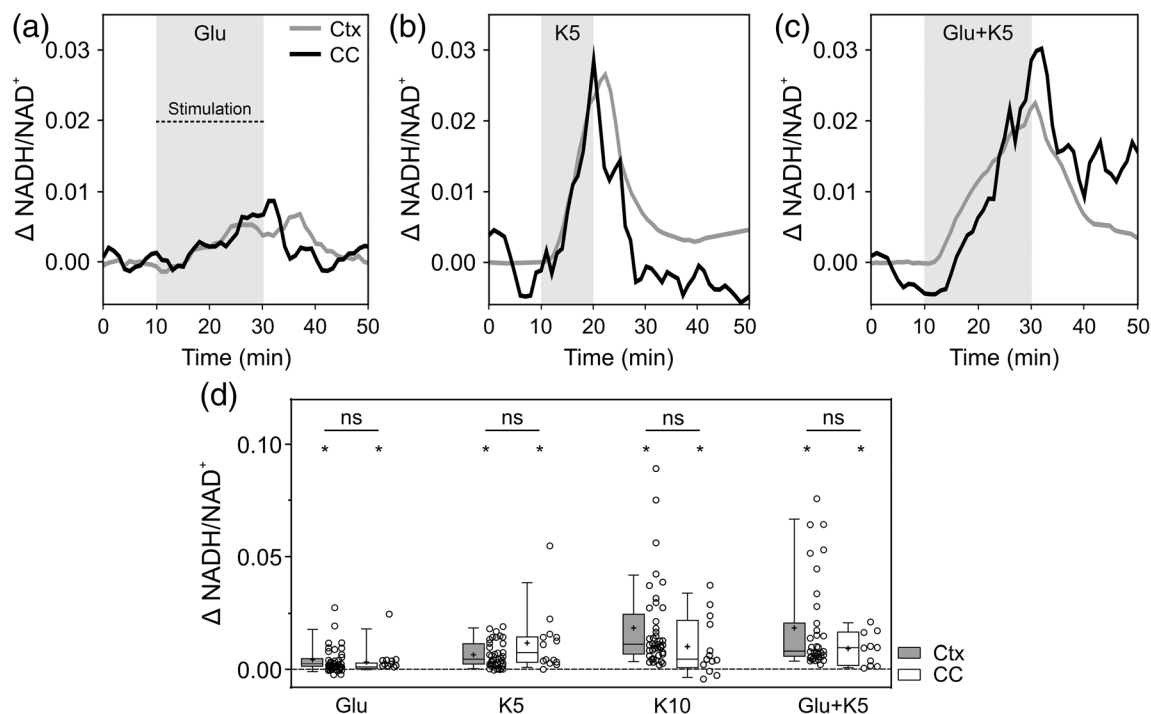
FIGURE 3 Glutamate and K^+ regulate the cytosolic NADH/NAD$^+$ redox state in astrocytes in gray and white matter. (a) Time course of the change of the NADH/NAD$^+$ redox ratio (ΔNADH/NAD$^+$ = NADH/NAD^+_t − NADH/NAD$^+_{baseline}$) in astrocytes in Ctx (gray line) and CC (black line) exposed to glutamate (100 µM; 20 min starting at 10 min of incubation as indicated by the gray shading). In (a–c) example traces are shown. (b) Time course of ΔNADH/NAD$^+$ in astrocytes exposed to potassium (5 mM; 10 min). (c) Time course of ΔNADH/NAD$^+$ in astrocytes exposed to glutamate (100 µM) and potassium (5 mM) for 20 min as indicated. (d) Quantification of ΔNADH/NAD$^+$ of astrocytes in Ctx (gray boxes) and CC (white boxes). The figure shows data averaged between 8 and 10 min after the onset of stimulation with glutamate (Glu; 100 µM), K^+ (K5: 5 mM; K10: 10 mM) or glutamate + K^+ (Glu + K5; 100 µM, 5 mM). Peredox was imaged by ratiometric 2-photon intensity imaging, data is given as difference to the NADH/NAD$^+$ redox ratio prior to stimulation in all panels. *Data set is significant different from baseline obtained before application of the respective treatment ($p < .05$). ns, no statistically significant difference between the conditions indicated ($p > .05$). For number of cells (n) and animals (N) see Table 1. Next to each boxplot, the same data set is presented as a dot plot showing all individual data points

For further experiments, ratiometric fluorescence intensity was measured instead of fluorescence lifetimes for several reasons: (1) FLIM measurements required a higher fluorescence intensity causing phototoxic damage over time especially in astrocytes in CC (Shannon et al., 2007; own observations) and are therefore no suitable method for long-lasting experiments. (2) Data obtained with both methods reveal a similar detection range and a similar basal redox state (compare Figure 2c,d) confirming that both methods generate reliable results.

Astrocytes sense neuronal activity and respond to activity levels, for example, by adjusting their metabolism allowing maintenance of brain energy homeostasis (Köhler et al., 2018; Pellerin & Magistretti, 1994; Sotelo-Hitschfeld et al., 2015; Zuend et al., 2020). Two signals related to neuronal activity are glutamate (released at excitatory, glutamatergic synapses as well as from active axons; Gasic & Hollmann, 1992; Kukley et al., 2007; Ziskin et al., 2007) and increased concentrations of extracellular potassium ([K^+]$_e$; released from neurons during repolarization; Poolos et al., 1987; Rash, 2010). Therefore, to investigate whether GM and WM astrocytes differ in their metabolic reactions in response to these two correlates of neuronal activity, the NADH/NAD$^+$ redox state was monitored.

Experiments were performed in the presence of TTX to prevent neuronal action potential firing allowing to study action potential-independent effects on astrocytes. TTX by itself had no effect on the NADH/NAD$^+$ redox state (Figure S2A). Application of glutamate induced a slow increase of the NADH/NAD$^+$ redox ratio, that is, a more reduced redox state in astrocytes both in the Ctx and CC (Figure 3a,d; note that data is given as ΔNADH/NAD$^+$, that is, NADH/NAD$^+_{baseline}$ was subtracted from NADH/NAD^+_t to highlight treatment induced changes). In contrast, the NADH/NAD$^+$ redox state increased much faster and more strongly when [K^+]$_e$ was increased (Figure 3b,d). Simultaneous application of both signals resulted in an additive increase of the NADH/NAD$^+$ redox state in Ctx, but not in CC (Figure 3c,d; Ctx: Glu vs. Glu + K5: $p < .05$, K5 vs. Glu + K5: $p < .05$; CC: Glu vs. Glu + K5: $p > .05$, K5 vs. Glu + K5: $p > .05$; nested ANOVA). Of note, despite the different basal NADH/NAD$^+$ redox state (Figure 2c,d), the change in the NADH/NAD$^+$ redox state induced by glutamate and increasing [K^+]$_e$ was not significantly different between astrocytes in Ctx and CC in all conditions tested (Figure 3d).

In addition to the NADH/NAD$^+$ redox state, the dynamics of the cytosolic concentration of ATP was analyzed in astrocytes in Ctx and
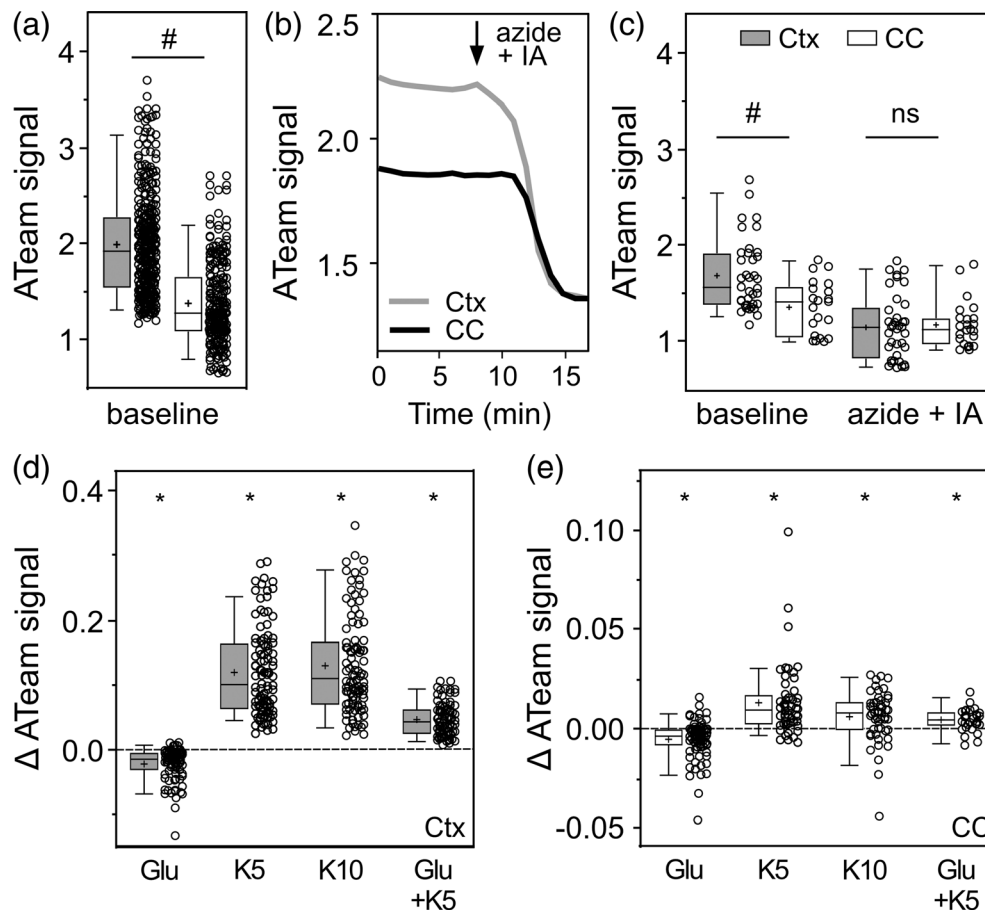
FIGURE 4 The baseline ATeam signal in gray and white matter astrocytes is different and regulated by glutamate and potassium. (a) The ATeam signal in cortical astrocytes (gray box) and astrocytes of corpus callosum (white box) under baseline condition (aCSF, 10 mM glucose) indicates a lower cytosolic concentration of ATP in astrocytes in CC compared to astrocytes in Ctx. (b) Example traces of the ATeam signal in astrocytes in Ctx (gray trace) and CC (black trace) before and after application (arrow) of azide (10 mM) and iodoacetate (IA; 1 mM) to deplete the cells of ATP. (c) Quantification of the baseline ATeam signal and the ATeam signal after depletion of ATP by application of azide + IA. Only cells were included in this analysis, for which both a stable baseline signal and a stable signal after azide + IA was obtained. (d) Quantification of the change of the ATeam fluorescence signal, that is, the difference to the ATeam signal prior to stimulation (ΔATeam signal = ATeam signal$_t$ − ATeam signal$_{baseline}$) in cortical astrocytes exposed to glutamate (Glu; 100 μM), potassium (K5: 5 mM; K10: 10 mM) and glutamate + potassium (Glu + K5; 100 μM, 5 mM). (e) Same experiment as in (d) for astrocytes in the corpus callosum. ATeam was imaged by ratiometric 2-photon intensity imaging. *Data set is significant different from baseline obtained before application of the respective treatment ($p < .05$). Significance of the difference between the conditions are indicated ($^\#p < .05$; ns: $p > .05$). For number of cells (n) and animals (N) see Table 1. Next to each boxplot, the same data set is presented as a dot plot showing all individual data points

CC taking advantage of the ATP sensor ATeam (Imamura et al., 2009). Under baseline conditions, the sensor signal, assessed as the ratio of the fluorescence intensity of its two fluorophores, was significantly lower in astrocytes in CC compared to astrocytes in Ctx indicating a lower concentration of ATP (Figure 4a). At the end of the experiments, sodium azide and iodoacetate were applied to block oxidative phosphorylation and glycolysis, respectively, thereby depleting the cells of ATP (Figure 4b,c). Only a subset of cells could be analyzed under these conditions due to swelling of the slice induced by azide + iodoacetate. However, also this subset showed the same difference of the baseline ATeam signal between astrocytes in Ctx and CC as the complete data set (Figure 4c). After depletion of ATP, no differences of the ATeam signal of astrocytes in Ctx and CC were observed, suggesting that the sensor behaves similar in the two

populations of cells. Therefore, the difference in the ATeam signal under baseline conditions very likely reflects a difference in basal [ATP]. However, due to the difficulties to calibrate the ATP sensor in situ, the ATeam signal could not be converted into ATP concentration. Consequently, because of the different baseline ATP sensor signal and the non-linearity of the sensor, quantitative comparisons of changes of the ATP concentration are only applicable within one cell population (e.g., Ctx baseline vs. Ctx treatment), but not between the two cell populations (i.e., Ctx vs. CC) (see Köhler et al., 2020 for a detailed discussion of the implications of different basal sensor signals).

In cortical astrocytes, application of glutamate induced a decrease in the ATeam signal, while increasing [K$^+$]$_e$ to 5 or 10 mM resulted in an increase in the ATP sensor signal (Figure 4d; note that data is given
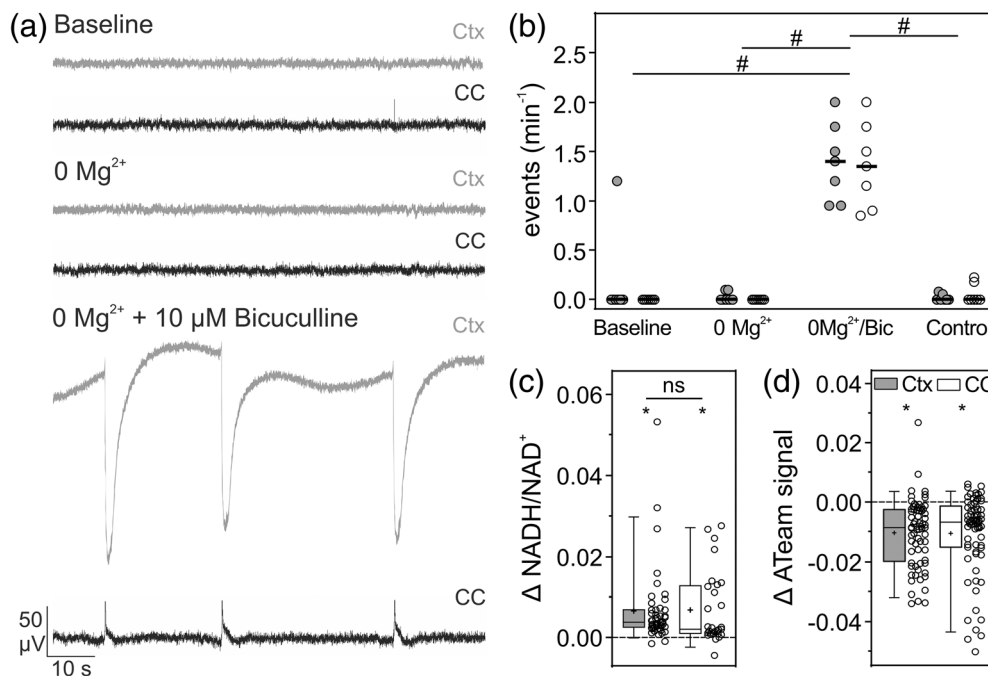
FIGURE 5 Intense, intrinsic neuronal activity affects cytosolic NADH/NAD$^+$ redox state and ATP of astrocytes in both Ctx and CC. (a) Simultaneous local field potential recordings of cortex (Ctx, gray) and corpus callosum (CC, black) under baseline condition, removal of Mg^{2+} (0 Mg^{2+}) and 0 Mg^{2+} + 10 μM bicuculline. Shown are example traces for both regions and each condition. Note the epileptiform discharges in the lower two traces. (b) Count of epileptiform depolarizations per minute. Control recordings were performed by incubating slices for 50 min under baseline conditions. Dots represent individual experiments (Ctx: gray dots; CC: white dots), black lines represent the median. (c) Quantification of the change of the NADH/NAD$^+$ redox ratio (ΔNADH/NAD$^+$) in astrocytes in Ctx (gray boxes) and CC (white boxes) within a time window of 2 min after 10 min stimulation with 0 Mg^{2+} + 10 μM bicuculline. Data is given as ΔNADH/NAD$^+$, that is, the difference to the NADH/NAD$^+$ redox ratio prior to stimulation. (d) Quantification of the change of the ATeam sensor fluorescence signal (ΔATeam) in astrocytes in Ctx and CC (same conditions as in c). *Data set is significant different from baseline ($p < .05$). Significance of the difference between the conditions are indicated ($^\#p < .05$; ns: $p > .05$). For number of cells (n) and animals (N) see Table 1. Next to each boxplot, the same data set is presented as a dot plot showing all individual data points

as ΔATeam signal). Strikingly, co-application of glutamate and increased [K$^+$]$_e$ (5 mM) resulted in an intermediate increase in the ATeam signal, suggesting that the increase in [ATP] induced by increasing [K$^+$]$_e$ compensates for the glutamate induced decrease (Figure 4d; Glu vs. Glu + K5: $p < .05$, K5 vs. Glu + K5: $p < .05$; nested ANOVA). These experiments were performed in the presence of TTX to exclude indirect effects caused by neuronal action potentials. Application of TTX alone had no effect on the ATeam signal in astrocytes from both Ctx and CC (Figure S2B). In astrocytes in the CC, glutamate application also resulted in a decrease of the ATeam signal, while increasing [K$^+$]$_e$ as well as co-application of glutamate and K$^+$ slightly increased it (Figure 4e). Taken together, these results indicate that the energy metabolism of astrocytes in both Ctx and CC is sensitive to glutamate and K$^+$ showing a similar pattern of response.

To study the metabolic dynamics of gray and white matter astrocytes during intrinsic neuronal activity, electrical activity in brain slices was induced by application of bicuculline and removal of Mg^{2+}. This treatment antagonizes inhibitory GABA$_A$ receptors and removes the Mg^{2+}-block of NMDA-type glutamate receptors, respectively, thereby inducing repetitive, supraphysiological neuronal depolarizations (Curtis et al., 1970; Karus et al., 2015). Epileptiform depolarizations

were observed almost simultaneously in Ctx and CC under these conditions within 5–7 min by local field potential recordings, while almost no such events occurred in baseline conditions or during removal of Mg^{2+} alone (Figure 5a,b). To confirm that these effects are not caused by prolonged recordings, experiments were repeated incubating the slices for 50 min under baseline conditions (i.e., the full duration of the previous experiment). Only very few depolarizations were observed in these control experiments (Figure 5b, Figure S3) indicating that the depolarizations observed are specifically induced by application of 0 Mg^{2+}/bicuculline.

Using this model of intense neuronal activity, the NADH/NAD$^+$ redox state and the cytosolic ATP were analyzed in astrocytes in Ctx and CC by monitoring the signals of Peredox and ATeam (Figure 5c,d). Neuronal activity induced a shift to a more reduced NADH/NAD$^+$ redox state both in astrocytes in the Ctx and CC, and the change in the NADH/NAD$^+$ redox state was not significantly different between the brain areas (Figure 5c). In parallel, the ATeam signal and hence cytosolic ATP levels decreased slightly in both cell populations (Figure 5d). Taken together, endogenous neuronal activity, in this model of intense, supraphysiological activation, results in metabolic regulation in astrocytes, with a

similar shift of the NADH/NAD$^+$ redox state in astrocytes in Ctx and CC.

4 | DISCUSSION

Astrocytes are a heterogeneous population of glial cells which differ in many properties between brain regions, but also within a given area of the brain (Bachoo et al., 2004; Ben Haim & Rowitch, 2017; Farmer & Murai, 2017; Hirrlinger & Nimmerjahn, 2022; Köhler et al., 2021; Matyash & Kettenmann, 2010; Miller, 2018; Oberheim et al., 2012; Schitine et al., 2015; Zhang & Barres, 2010). We here compared metabolic properties of astrocytes in the Ctx and CC, representative brain areas for GM and WM, respectively, focusing on the NADH/NAD$^+$ redox state and the cytosolic concentration of ATP. The NADH/NAD$^+$ redox ratio is a crucial metabolic node connecting pathways like glycolysis, lactate production, TCA cycle and respiratory chain. Furthermore, the NADH/NAD$^+$ redox ratio is also sensed by cellular signaling processes which are vice versa regulated by changes in the NADH/NAD$^+$ redox ratio (Berger et al., 2004; Hirrlinger & Dringen, 2010; Requardt et al., 2012; Rutter et al., 2001; Winkler & Hirrlinger, 2015; Ying, 2007). ATP is the central energy carrier of cells and glutamate uptake-induced changes in [ATP] have been suggested to regulate metabolic support from astrocytes to neurons (Azarias et al., 2011; Barros & Deitmer, 2010; Bolaños, 2016; Dienel, 2013). We show here that astrocytes in GM and WM differ in their basal NADH/NAD$^+$ redox state and ATP levels, which are sensitive to signals of neuronal activity in both astrocyte populations.

The basal NADH/NAD$^+$ redox state was more reduced in astrocytes in WM compared to GM. Of note, this observation was revealed with both fluorescence lifetime imaging and ratiometric intensity-based imaging, suggesting that the differences are most likely not artificially generated, for example, by different scattering properties of GM and WM, or by different scattering of light of the two wavelengths used for ratiometric imaging. As a note of caution, the quantification of the NADH/NAD$^+$ redox state relies on the assumption that saturation of the Peredox sensor is achieved during application of 10 mM lactate or pyruvate. While such a procedure has been used successfully in cultured cells before (Hung et al., 2011; Köhler et al., 2018; Mongeon et al., 2016), we cannot formally exclude that the calibration procedure is affected by issues of diffusion or uptake of lactate and pyruvate within the acute brain slice.

Fluorescent nanosensors report the actual concentration / redox ratio of the respective metabolite, but not underlying metabolic fluxes (Koveal et al., 2020). Some experimental paradigms have been developed to measure metabolic fluxes, for example, for glucose, lactate and pyruvate (Bittner et al., 2010; San Martín et al., 2013; San Martín, Ceballo, et al., 2014). However, in our experiments the nanosensors report the steady state levels of the NADH/NAD$^+$ redox state or cytosolic ATP. Therefore, the increased NADH/NAD$^+$ redox state in WM might be due to either a relatively higher production or lower consumption of NADH, while no conclusion on the overall rate of the metabolic flux in Ctx compared to CC can be obtained from these experiments. Similarly, the lower signal of the ATP sensor in WM astrocytes reflects a higher consumption or lower production of ATP. In general, glucose uptake, glucose phosphorylation and local glucose utilization is slower in WM compared to GM (Sokoloff et al., 1977), but whether this also refers to astrocytes specifically has not been clarified yet. Furthermore, glycogen content is higher in GM astrocytes compared to WM astrocytes albeit with regional differences (Brown, 2004; Brown & Ransom, 2007; Hirase et al., 2019; Oe et al., 2016; Sagar et al., 1987; Swanson et al., 1989). In GM, glycogen-derived lactate released from astrocytes supports glutamatergic neurotransmission (Bak & Walls, 2018; Dienel et al., 2007; Sickmann et al., 2009), while, for example, in the highly myelinated optic nerve, lactate produced from astrocytic glycogen is essential to maintain the electrical activity during periods with low availability of energy substrates and lactate transport is necessary for maintaining axonal ATP levels (Brown et al., 2005; Trevisiol et al., 2017; Wender et al., 2000). In the CC, glucose rather than lactate is transferred from oligodendrocytes to axons (Meyer et al., 2018). On the other hand, the activity of oxidative metabolism is lower than glycolytic activity in WM, suggesting that WM is more prone to produce lactate (Morland et al., 2007). While it has not been resolved whether this observation obtained in total WM tissue is specifically reflecting properties of astrocytes, an increase of glycolytic activity in combination with low lactate usage under basal conditions would be consistent with an increased NADH/NAD$^+$ redox state. Of note, even under the well-controlled basal experimental conditions providing glucose as energy substrate, the NADH/NAD$^+$ redox state shows a large variability between cells indicating a pronounced heterogeneity of basal energy metabolism in astrocytes as reported previously (Köhler et al., 2018; Mongeon et al., 2016). In addition, the consumption of ATP varies substantially depending on the physiological situation of a cell, thereby requiring adaptation of ATP production. We formally cannot exclude that the lower signal of the ATP sensor in astrocytes in CC is due to different properties of the ATeam sensor when expressed in WM astrocytes, including optical differences like enhanced scattering, biochemical (e.g., different binding constants, different pH) or biophysical properties (e.g., different lifetimes of the sensor), which could be caused by a different cellular environment or proteins interacting with the sensor in one cell type, but not the other (see Koveal et al. (2020) for a detailed discussion of confounding factors). However, the observation that the ATP sensor reveals the same signal in astrocytes in Ctx and CC after depletion of ATP shows that—at least under this condition—the ATP sensor behaves similar in both cell populations. Therefore, despite these caveats, these results suggest that the concentration of cytosolic ATP is lower in WM astrocytes compared to astrocytes in GM. Mechanistically, the high NADH/NAD$^+$ redox ratio and low ATP might be linked via soluble adenylate cyclase which—as shown in other cellular systems—is inhibited by low ATP (Zippin et al., 2013) and its inhibition results in an increased NADH/NAD$^+$ redox ratio (Chang et al., 2021). However, whether the reduced ATP level observed in astrocytes in the CC reflects a lower energy demand or a more constant ATP usage (thereby requiring less "reserve" ATP for peak demands) of WM astrocytes remains to be elucidated.

The local energy metabolism within the brain has to be adapted to the actual local energy need (Oheim et al., 2018). Astrocytes are key players in this neurometabolic coupling given their strategic position contacting blood vessels, neuronal somata, synapses and axons (Allaman et al., 2011; Allen & Barres, 2009; Bolaños, 2016; Bonvento & Bolaños, 2021; Nortley & Attwell, 2017; Yi et al., 2011). Metabolism of astrocytes is regulated by signals indicating activity of neurons including glutamate and K^+. Glutamate is released at glutamatergic synapses, but also along axons propagating action potentials (Kukley et al., 2007; Wake et al., 2011; Ziskin et al., 2007). Glutamate can reach high concentrations in the vicinity of active synapses for very short times in the millisecond range. However, as a caveat, the experimental conditions used here (100 μM glutamate for minutes) are supraphysiological. K^+ is released from active neurons during repolarization (Rash, 2010). Both glutamate and increasing $[K^+]_e$ induced an increase of the $NADH/NAD^+$ redox ratio in cortical astrocytes consistent with previous reports indicating activation of glycolysis by these signals (Bittner et al., 2010; Bittner et al., 2011; Fernandez-Moncada et al., 2018; Ruminot et al., 2011; Sotelo-Hitschfeld et al., 2012, 2015). Glutamate and increasing $[K^+]_e$ stimulate glycolysis in astrocytes with different kinetics (Bittner et al., 2011; Köhler et al., 2018), which is reflected in the different kinetics and amplitudes of the change of the $NADH/NAD^+$ redox ratio. Of note, both correlates of neuronal activity together resulted in an additive response of the $NADH/NAD^+$ redox ratio, suggesting that they synergistically activate astrocytic energy metabolism, including glycolysis.

The ATP sensor signal was also modulated by the application of glutamate and increasing $[K^+]_e$. In cortical astrocytes, application of glutamate resulted in a decrease of [ATP], consistent with previous observations in other experimental systems (Fernandez-Moncada et al., 2018; Magistretti & Chatton, 2005; Winkler et al., 2017). In cultured cortical astrocytes, this decrease was estimated as −0.16 mM or −11% of basal [ATP] (Köhler et al., 2020). In contrast, increasing $[K^+]_e$ from 2.5 to 5 mM (or 10 mM), which is well within the range of physiological changes of $[K^+]_e$ (Kofuji & Newman, 2004), induced an increase in the ATP sensor signal indicating that ATP production is enhanced or ATP consumption reduced (Fernandez-Moncada et al., 2018; Lerchundi et al., 2019). In cultured cortical astrocytes, this increase was quantified as 0.07 mM, that is, 5% of basal [ATP] (Köhler et al., 2020). Increasing $[K^+]_e$ results in activation of astrocyte glycolytic metabolism by a mechanism involving the sodium-bicarbonate cotransporter NBCe1, alkalization of the cytosol, and soluble adenylate cyclase (Choi et al., 2012; MacVicar & Choi, 2017), providing a potential mechanism for the increased $NADH/NAD^+$ redox ratio and ATP production. Consistent with the additive increase of the $NADH/NAD^+$ redox ratio, the decrease of ATP induced by application of glutamate alone was compensated by simultaneously increasing $[K^+]_e$ even under the supraphysiogical conditions of stimulation by glutamate, indicating a very pronounced activation of ATP producing metabolic pathways. Several mechanisms might underlie this observation: (a) the glutamate induced decrease in cytosolic pH in astrocytes is turned into alkalization by simultaneously increasing $[K^+]_e$ (Rimmele

et al., 2018), thereby enabling stimulation of ATP production mediated by soluble adenylate cyclase (Choi et al., 2012; MacVicar & Choi, 2017); (b) increased $[K^+]_e$ inhibits glutamate transport (Rimmele et al., 2017; Tyurikova et al., 2022), thereby reducing glutamate-induced acidification as well as Na^+/K^+-ATPase dependent ATP demand. Furthermore, whether the non-canonical control of ATP production by Na^+/K^+-ATPase recently described for neurons (Baeza-Lehnert et al., 2019) also contributes to regulation of metabolism in astrocytes remains to be established.

The CC, a typical WM region of the brain, has very different properties and functions compared to Ctx, a typical GM region. In Ctx, synapses are the main source of glutamate, and K^+ is released from active dendrites, neuronal somata and axons. In the WM, glutamate is released only from axons, albeit at lower amounts than in GM (Kukley et al., 2007; Wake et al., 2011; Ziskin et al., 2007), and axons release K^+ during repolarization (Rash, 2010). Furthermore, action potential propagation in WM demands different energetic needs than synaptic signal transmission and integration. Nevertheless, astrocytes in CC showed a similar metabolic response as cortical astrocytes to bath application of glutamate, increased $[K^+]_e$ or a combination of both treatments. Furthermore, astrocytes only have direct access to either unmyelinated axons or limited to the node of Ranvier. Glutamate is taken up by astrocytes via the glutamate transporters GLAST or Glt-1 (Rose et al., 2018). GLAST-promoter activity has been detected in WM astrocytes in the adult mouse brain; however, expression and activity of the glutamate transporter Glt-1 is markedly lower in WM astrocytes compared to GM (Hassel et al., 2003; Regan et al., 2007). Furthermore, in WM also oligodendrocytes contribute to metabolic support and ion homeostasis (Fünfschilling et al., 2012; Hirrlinger & Nave, 2014; Lee et al., 2012; Nave, 2010a, 2010b; Rash, 2010) and glutamate released from axons regulates metabolic support from oligodendrocytes to axons via oligodendroglial NMDA-receptors (Saab et al., 2016). However, our data indicate that these potential differences in metabolic demands for astrocytes in Ctx and CC are mainly reflected in differences in basal regulation of metabolism, but the mechanisms responding to neuronal activity are conserved between the two brain regions.

A decrease in [ATP] induced by glutamate uptake has been proposed as a major mechanism of neuron-astrocyte metabolic coupling in GM (Azarias et al., 2011; Barros & Deitmer, 2010; Bolaños, 2016; Dienel, 2013; Pellerin & Magistretti, 2012). During neuronal activity, K^+ is necessarily released as well (Poolos et al., 1987; Rash, 2010) raising the possibility that [ATP] rather increases also in more physiological situations because of K^+ induced metabolic stimulation. However, when high intrinsic electrical activity was induced in slices by $0\ Mg^{2+}$/bicuculline, a slight reduction in the ATP sensor signal in astrocytes in Ctx and CC was observed, suggesting that the K^+ induced increase in [ATP] cannot fully compensate the activity induced increase in ATP consumption under these conditions. A biphasic response of astrocytic [ATP] consisting of a short increase followed by a prolonged decrease below basal levels was reported in hippocampal organotypic cultures during treatment with $0\ Mg^{2+}$/bicuculline (Lerchundi et al., 2020). Within the GM of the brain,

astrocytes extend uncountable fine processes contacting numerous synapses and forming local microdomains (Aten et al., 2022; Grosche et al., 1999; Reichenbach et al., 2010). Subcellular regulation of astrocytic metabolism on the spatial scale of these microdomains has been proposed (Oheim et al., 2018). It is tempting to speculate that in astroglial processes, which are in close contact to glutamatergic synapses, a decrease of [ATP] by glutamate prevails, while other parts of the cells might be mainly affected by fluctuations of $[K^+]_e$. Glutamate uptake also varies between single synapses depending on the spine size (Herde et al., 2020). A similar situation might reflect astrocyte processes contacting the nodes of Ranvier in WM. However, detailed knowledge of the concentration of glutamate and K^+ during physiological brain function at high temporal and spatial resolution is currently lacking, therefore, the details of such subcellular regulation remain to be established.

In summary, we have compared metabolic properties of astrocytes in the Ctx and CC, two prototypical brain regions for GM and WM, respectively. We provide evidence that astrocytes in both regions have different basal metabolic properties, but respond metabolically to neuronal activity in a similar pattern. Therefore, these findings provide novel insight in metabolic homeostasis of the brain and add to the increasing knowledge of heterogeneity of astrocytes within different brain regions (Farmer & Murai, 2017; García-Marqués & López-Mascaraque, 2013; Hirrlinger & Nimmerjahn, 2022; Köhler et al., 2021; Matyash & Kettenmann, 2010; Zhang & Barres, 2010).

AUTHOR CONTRIBUTIONS

ACKNOWLEDGMENTS

DATA AVAILABILITY STATEMENT

All datasets generated and analyzed for this study are included in the manuscript and the supplementary files.

ORCID

Susanne Köhler https://orcid.org/0000-0001-6895-6998
Kristina Lippmann https://orcid.org/0000-0001-7719-0437
Jens Eilers https://orcid.org/0000-0003-0497-5625
Johannes Hirrlinger https://orcid.org/0000-0002-6327-0089

REFERENCES

Aberg, F., & Kozlova, E. N. (2000). Metastasis-associated mts1 (S100A4) protein in the developing and adult central nervous system. *Journal of Comparative Neurology*, *424*(2), 269–282. https://doi.org/10.1002/1096-9861(20000821)424:2<269::AID-CNE6>3.0.CO;2-M

Allaman, I., Bélanger, M., & Magistretti, P. J. (2011). Astrocyte-neuron metabolic relationships: For better and for worse. *Trends in Neurosciences*, *34*(2), 76–87. https://doi.org/10.1016/j.tins.2010.12.001

Allen, N. J., & Barres, B. A. (2009). Glia – More than just brain glue. *Nature Neuroscience*, *457*(7230), 675–677. https://doi.org/10.1038/457675a

Araque, A., Parpura, V., Sanzgiri, R. P., & Haydon, P. G. (1999). Tripartite synapses: Glia, the unacknowledged partner. *Trends in Neurosciences*, *22*(5), 208–215. https://doi.org/10.1016/S0166-2236(98)01349-6

Aten, S., Kiyoshi, C. M., Arzola, E. P., Patterson, J. A., Taylor, A. T., Du, Y., Guiher, A. M., Philip, M., Camacho, E. G., Mediratta, D., Collins, K., Boni, K., Garcia, S. A., Kumar, R., Drake, A. N., Hegazi, A., Trank, L., Benson, E., Kidd, G., … Zhou, M. (2022). Ultrastructural view of astrocyte arborization, astrocyte-astrocyte and astrocyte-synapse contacts, intracellular vesicle-like structures, and mitochondrial network. *Progress in Neurobiology*, *213*, 102264. https://doi.org/10.1016/j.pneurobio.2022.102264

Azarias, G., Perreten, H., Lengacher, S., Poburko, D., Demaurex, N., Magistretti, P. J., & Chatton, J.-Y. (2011). Glutamate transport decreases mitochondrial pH and modulates oxidative metabolism in astrocytes. *Journal of Neuroscience*, *31*(10), 3550–3559. https://doi.org/10.1523/JNEUROSCI.4378-10.2011

Bachoo, R. M., Kim, R. S., Ligon, K. L., Maher, E. A., Brennan, C., Billings, N., Chan, S., Li, C., Rowitch, D. H., Wong, W. H., & DePinho, R. A. (2004). Molecular diversity of astrocytes with implications for neurological disorders. *Proceedings of the National Academy of Sciences of the United States of America*, *101*(22), 8384–8389. https://doi.org/10.1073/pnas.0402140101

Baeza-Lehnert, F., Saab, A. S., Gutierrez, R., Larenas, V., Diaz, E., Horn, M., Vargas, M., Hosli, L., Stobart, J., Hirrlinger, J., Weber, B., & Barros, L. F. (2019). Non-canonical control of neuronal energy status by the Na^+ pump. *Cell Metabolism*, *29*(3), 668–680. https://doi.org/10.1016/j.cmet.2018.11.005

Bak, L. K., Schousboe, A., & Waagepetersen, H. S. (2006). The glutamate/GABA-glutamine cycle: Aspects of transport, neurotransmitter homeostasis and ammonia transfer. *Journal of Neurochemistry*, *98*(3), 641–653. https://doi.org/10.1111/j.1471-4159.2006.03913.x

Bak, L. K., & Walls, A. B. (2018). Crosstalk opposing view: Lack of evidence supporting an astrocyte-to-neuron lactate shuttle coupling neuronal activity to glucose utilisation in the brain. *Journal of Physiology*, *596*(3), 351–353. https://doi.org/10.1113/JP274945

Barros, L. F., & Deitmer, J. W. (2010). Glucose and lactate supply to the synapse. *Brain Research Reviews*, *63*(1–2), 149–159. https://doi.org/10.1016/j.brainresrev.2009.10.002

Ben Haim, L., & Rowitch, D. H. (2017). Functional diversity of astrocytes in neural circuit regulation. *Nature Reviews Neuroscience*, *18*(1), 31–41. https://doi.org/10.1038/nrn.2016.159

Benjamin, A. M., & Quastel, J. H. (1974). Fate of L-glutamate in the brain. *Journal of Neurochemistry*, *23*(3), 457–464. https://doi.org/10.1111/j.1471-4159.1974.tb06046.x

Berger, F., Ramírez-Hernández, M. H., & Ziegler, M. (2004). The new life of a centenarian: Signalling functions of NAD(P). *Trends in Biochemical Sciences*, *29*(3), 111–118. https://doi.org/10.1016/j.tibs.2004.01.007

Bignami, A., Eng, L. F., Dahl, D., & Uyeda, C. T. (1972). Localization of the glial fibrillary acidic protein in astrocytes by immunofluorescence. *Brain Research*, *43*(2), 429–435. https://doi.org/10.1016/0006-8993(72)90398-8

Bittner, C. X., Loaiza, A., Ruminot, I., Larenas, V., Sotelo-Hitschfeld, T., Gutiérrez, R., Córdova, A., Valdebenito, R., Frommer, W. B., & Barros, L. F. (2010). High resolution measurement of the glycolytic

rate. *Frontiers in Neuroenergetics*, *2*, 26. https://doi.org/10.3389/fnene.2010.00026

Bittner, C. X., Valdebenito, R., Ruminot, I., Loaiza, A., Larenas, V., Sotelo-Hitschfeld, T., Moldenhauer, H., San Martín, A., Gutiérrez, R., Zambrano, M., & Barros, L. F. (2011). Fast and reversible stimulation of astrocytic glycolysis by K^+ and a delayed and persistent effect of glutamate. *Journal of Neuroscience*, *31*(12), 4709–4713. https://doi.org/10.1523/JNEUROSCI.5311-10.2011

Bolaños, J. P. (2016). Bioenergetics and redox adaptations of astrocytes to neuronal activity. *Journal of Neurochemistry*, *139*(Suppl. 2), 115–125. https://doi.org/10.1111/jnc.13486

Bonvento, G., & Bolaños, J. P. (2021). Astrocyte-neuron metabolic cooperation shapes brain activity. *Cell Metabolism*, *33*(8), 1546–1564. https://doi.org/10.1016/j.cmet.2021.07.006

Bribián, A., Figueres-Oñate, M., Martín-López, E., & López-Mascaraque, L. (2016). Decoding astrocyte heterogeneity: New tools for clonal analysis. *Neuroscience*, *323*, 10–19. https://doi.org/10.1016/j.neuroscience.2015.04.036

Brown, A. M. (2004). Brain glycogen re-awakened. *Journal of Neurochemistry*, *89*(3), 537–552. https://doi.org/10.1111/j.1471-4159.2004.02421.x

Brown, A. M., & Ransom, B. R. (2007). Astrocyte glycogen and brain energy metabolism. *Glia*, *55*(12), 1263–1271. https://doi.org/10.1002/glia.20557

Brown, A. M., Sickmann, H. M., Fosgerau, K., Lund, T. M., Schousboe, A., Waagepetersen, H. S., & Ransom, B. R. (2005). Astrocyte glycogen metabolism is required for neural activity during aglycemia or intense stimulation in mouse white matter. *Journal of Neuroscience Research*, *79*(1–2), 74–80. https://doi.org/10.1002/jnr.20335

Chang, J.-C., Go, S., Gilglioni, E. H., Duijst, S., Panneman, D. M., Rodenburg, R. J., Li, H. L., Huang, H.-L., Levin, L. R., Buck, J., Verhoeven, A. J., & Oude Elferink, R. P. J. (2021). Soluble adenylyl cyclase regulates the cytosolic $NADH/NAD^+$ redox state and the bioenergetic switch between glycolysis and oxidative phosphorylation. *Biochimica et Biophysica Acta: Bioenergetics*, *1862*(4), 148367. https://doi.org/10.1016/j.bbabio.2020.148367

Choi, H. B., Gordon, G. R. J., Zhou, N., Tai, C., Rungta, R. L., Martinez, J., Milner, T. A., Ryu, J. K., McLarnon, J. G., Tresguerres, M., Levin, L. R., Buck, J., & MacVicar, B. A. (2012). Metabolic communication between astrocytes and neurons via bicarbonate-responsive soluble adenylyl cyclase. *Neuron*, *75*(6), 1094–1104. https://doi.org/10.1016/j.neuron.2012.08.032

Curtis, D. R., Duggan, A. W., Felix, D., & Johnston, G. A. (1970). GABA, bicuculline and central inhibition. *Nature*, *226*(5252), 1222–1224. https://doi.org/10.1038/2261222a0

Díaz-García, C. M., Mongeon, R., Lahmann, C., Koveal, D., Zucker, H., & Yellen, G. (2017). Neuronal stimulation triggers neuronal glycolysis and not lactate uptake. *Cell Metabolism*, *26*(2), 361–374. https://doi.org/10.1016/j.cmet.2017.06.021

Dienel, G. A. (2013). Astrocytic energetics during excitatory neurotransmission: What are contributions of glutamate oxidation and glycolysis? *Neurochemistry International*, *63*(4), 244–258. https://doi.org/10.1016/j.neuint.2013.06.015

Dienel, G. A., Ball, K. K., & Cruz, N. F. (2007). A glycogen phosphorylase inhibitor selectively enhances local rates of glucose utilization in brain during sensory stimulation of conscious rats: Implications for glycogen turnover. *Journal of Neurochemistry*, *102*(2), 466–478. https://doi.org/10.1111/j.1471-4159.2007.04595.x

DiNuzzo, M., Mangia, S., Maraviglia, B., & Giove, F. (2012). The role of astrocytic glycogen in supporting the energetics of neuronal activity. *Neurochemical Research*, *37*(11), 2432–2438. https://doi.org/10.1007/s11064-012-0802-5

Farhy-Tselnicker, I., & Allen, N. J. (2018). Astrocytes, neurons, synapses: A tripartite view on cortical circuit development. *Neural Development*, *13*(1), 1–12. https://doi.org/10.1186/s13064-018-0104-y

Farmer, W. T., & Murai, K. (2017). Resolving astrocyte heterogeneity in the CNS. *Frontiers in Cellular Neuroscience*, *11*, 1–7. https://doi.org/10.3389/fncel.2017.00300

Fern, R., Davis, P., Waxman, S. G., & Ransom, B. R. (1998). Axon conduction and survival in CNS white matter during energy deprivation: A developmental study. *Journal of Neurophysiology*, *79*(1), 95–105. https://doi.org/10.1152/jn.1998.79.1.95

Fernandez-Moncada, I., Ruminot, I., Robles-Maldonado, D., Alegria, K., Deitmer, J. W., & Barros, L. F. (2018). Neuronal control of astrocytic respiration through a variant of the Crabtree effect. *Proceedings of the National Academy of Sciences of the United States of America*, *115*(7), 1623–1628. https://doi.org/10.1073/pnas.1716469115

Fünfschilling, U., Supplie, L. M., Mahad, D., Boretius, S., Saab, A. S., Edgar, J., Brinkmann, B. G., Kassmann, C. M., Tzvetanova, I. D., Möbius, W., Diaz, F., Meijer, D., Suter, U., Hamprecht, B., Sereda, M. W., Moraes, C. T., Frahm, J., Goebbels, S., & Nave, K.-A. (2012). Glycolytic oligodendrocytes maintain myelin and long-term axonal integrity. *Nature*, *485*(7399), 517–521. https://doi.org/10.1038/nature11007

García-Marqués, J., & López-Mascaraque, L. (2013). Clonal identity determines astrocyte cortical heterogeneity. *Cerebral Cortex*, *23*(6), 1463–1472. https://doi.org/10.1093/cercor/bhs134

Gasic, G. P., & Hollmann, M. (1992). Molecular neurobiology of glutamate receptors. *Annual Review of Physiology*, *54*, 507–536. https://doi.org/10.1146/annurev.ph.54.030192.002451

Grosche, J., Matyash, V., Moller, T., Verkhratsky, A., Reichenbach, A., & Kettenmann, H. (1999). Microdomains for neuron-glia interaction: parallel fiber signaling to Bergmann glial cells. *Nature Neuroscience*, *2*(2), 139–143. https://doi.org/10.1038/5692

Hamner, M. A., Moller, T., & Ransom, B. R. (2011). Anaerobic function of CNS white matter declines with age. *Journal of Cerebral Blood Flow & Metabolism*, *31*(4), 996–1002. https://doi.org/10.1038/jcbfm.2010.216

Hassel, B., Boldingh, K. A., Narvesen, C., Iversen, E. G., & Skrede, K. K. (2003). Glutamate transport, glutamine synthetase and phosphate-activated glutaminase in rat CNS white matter. A quantitative study. *Journal of Neurochemistry*, *87*(1), 230–237. https://doi.org/10.1046/j.1471-4159.2003.01984.x

Herde, M. K., Bohmbach, K., Domingos, C., Vana, N., Komorowska-Müller, J. A., Passlick, S., Schwarz, I., Jackson, C. J., Dietrich, D., Schwarz, M. K., & Henneberger, C. (2020). Local efficacy of glutamate uptake decreases with synapse size. *Cell Reports*, *32*(12), 108182. https://doi.org/10.1016/j.celrep.2020.108182

Hertz, L., & Zielke, H. R. (2004). Astrocytic control of glutamatergic activity: Astrocytes as stars of the show. *Trends in Neurosciences*, *27*(12), 735–743. https://doi.org/10.1016/j.tins.2004.10.008

Hirase, H., Akther, S., Wang, X., & Oe, Y. (2019). Glycogen distribution in mouse hippocampus. *Journal of Neuroscience Research*, *97*(8), 923–932. https://doi.org/10.1002/jnr.24386

Hirrlinger, J., & Dringen, R. (2010). The cytosolic redox state of astrocytes: Maintenance, regulation and functional implications for metabolite trafficking. *Brain Research Reviews*, *63*(1–2), 177–188. https://doi.org/10.1016/j.brainresrev.2009.10.003

Hirrlinger, J., & Nave, K.-A. (2014). Adapting brain metabolism to myelination and long-range signal transduction. *Glia*, *62*(11), 1749–1761. https://doi.org/10.1002/glia.22737

Hirrlinger, J., & Nimmerjahn, A. (2022). A perspective on astrocyte regulation of neural circuit function and animal behavior. *Glia*, *70*(8), 1554–1580. https://doi.org/10.1002/glia.24168

Hung, Y. P., Albeck, J. G., Tantama, M., & Yellen, G. (2011). Imaging cytosolic $NADH-NAD^+$ redox state with a genetically encoded fluorescent biosensor. *Cell Metabolism*, *14*(4), 545–554. https://doi.org/10.1016/j.cmet.2011.08.012

Hung, Y. P., & Yellen, G. (2014). Live-cell imaging of cytosolic $NADH-NAD^+$ redox state using a genetically encoded fluorescent

biosensor. *Methods in Molecular Biology*, 1071, 83–95. https://doi.org/10.1007/978-1-62703-622-1_7

Imamura, H., Nhat, K. P., Togawa, H., Saito, K., Iino, R., Kato-Yamada, Y., Nagai, T., & Noji, H. (2009). Visualization of ATP levels inside single living cells with fluorescence resonance energy transfer-based genetically encoded indicators. *Proceedings of the National Academy of Sciences*, 106(37), 15651–15656. https://doi.org/10.1073/pnas.0904764106

Karus, C., Mondragao, M. A., Ziemens, D., & Rose, C. R. (2015). Astrocytes restrict discharge duration and neuronal sodium loads during recurrent network activity. *Glia*, 63(6), 936–957. https://doi.org/10.1002/glia.22793

Kofuji, P., & Newman, E. A. (2004). Potassium buffering in the central nervous system. *Neuroscience*, 129(4), 1045–1056. https://doi.org/10.1016/j.neuroscience.2004.06.008

Köhler, S., Schmidt, H., Fülle, P., Hirrlinger, J., & Winkler, U. (2020). A dual nanosensor approach to determine the cytosolic concentration of ATP in astrocytes. *Frontiers in Cellular Neuroscience*, 14, 1–14. https://doi.org/10.3389/fncel.2020.565921

Köhler, S., Winkler, U., & Hirrlinger, J. (2021). Heterogeneity of astrocytes in grey and white matter. *Neurochemical Research*, 46(1), 3–14. https://doi.org/10.1007/s11064-019-02926-x

Köhler, S., Winkler, U., Sicker, M., & Hirrlinger, J. (2018). Nbce1 mediates the regulation of the NADH/NAD$^+$ redox state in cortical astrocytes by neuronal signals. *Glia*, 66(10), 2233–2245. https://doi.org/10.1002/glia.23504

Koveal, D., Díaz-García, C. M., & Yellen, G. (2020). Fluorescent biosensors for neuronal metabolism and the challenges of quantitation. *Current Opinion in Neurobiology*, 63, 111–121. https://doi.org/10.1016/j.conb.2020.02.011

Kukley, M., Capetillo-Zarate, E., & Dietrich, D. (2007). Vesicular glutamate release from axons in white matter. *Nature Neuroscience*, 10(3), 311–320. https://doi.org/10.1038/nn1850

Lee, Y., Messing, A., Su, M., & Brenner, M. (2008). GFAP promoter elements required for region-specific and astrocyte-specific expression. *Glia*, 56(5), 481–493. https://doi.org/10.1002/glia.20622

Lee, Y., Morrison, B. M., Li, Y., Lengacher, S., Farah, M. H., Hoffman, P. N., Liu, Y., Tsingalia, A., Jin, L., Zhang, P.-W., Pellerin, L., Magistretti, P. J., & Rothstein, J. D. (2012). Oligodendroglia metabolically support axons and contribute to neurodegeneration. *Nature*, 487(7408), 443–448. https://doi.org/10.1038/nature11314

Lerchundi, R., Huang, N., & Rose, C. R. (2020). Quantitative imaging of changes in astrocytic and neuronal ATP using two different variants of ATeam. *Frontiers in Cellular Neuroscience*, 14, 1–13. https://doi.org/10.3389/fncel.2020.00080

Lerchundi, R., Kafitz, K. W., Winkler, U., Färfers, M., Hirrlinger, J., & Rose, C. R. (2019). FRET-based imaging of intracellular ATP in organotypic brain slices. *Journal of Neuroscience Research*, 97(8), 933–945. https://doi.org/10.1002/jnr.24361

Li, Y., Natakorn, S., Chen, Y., Safar, M., Cunningham, M., Tian, J., & Li, D. D.-U. (2020). Investigations on average fluorescence lifetimes for visualizing multi-exponential decays. *Frontiers in Physics*, 8, 447. https://doi.org/10.3389/fphy.2020.576862

Luskin, M. B., & McDermott, K. (1994). Divergent lineages for oligodendrocytes and astrocytes originating in the neonatal forebrain subventricular zone. *Glia*, 11(3), 211–226. https://doi.org/10.1002/glia.440110302

Mächler, P., Wyss, M. T., Elsayed, M., Stobart, J., Gutierrez, R., Faber-Castell, A. V., Kaelin, V., Zuend, M., San Martín, A., Romero-Gómez, I., Baeza-Lehnert, F., Lengacher, S., Schneider, B. L., Aebischer, P., Magistretti, P. J., Barros, L. F., & Weber, B. (2016). In vivo evidence for a lactate gradient from astrocytes to neurons. *Cell Metabolism*, 23(1), 94–102. https://doi.org/10.1016/j.cmet.2015.10.010

MacVicar, B. A., & Choi, H. B. (2017). Astrocytes provide metabolic support for neuronal synaptic function in response to extracellular K$^+$.

Neurochemical Research, 42(9), 2588–2594. https://doi.org/10.1007/s11064-017-2315-8

Magistretti, P. J., & Chatton, J.-Y. (2005). Relationship between L-glutamate-regulated intracellular Na$^+$ dynamics and ATP hydrolysis in astrocytes. *Journal of Neural Transmission*, 112(1), 77–85. https://doi.org/10.1007/s00702-004-0171-6

Matute, C., Domercq, M., Pérez-Samartín, A., & Ransom, B. R. (2013). Protecting white matter from stroke injury. *Stroke*, 44(4), 1204–1211. https://doi.org/10.1161/STROKEAHA.112.658328

Matyash, V., & Kettenmann, H. (2010). Heterogeneity in astrocyte morphology and physiology. *Brain Research Reviews*, 63(1–2), 2–10. https://doi.org/10.1016/j.brainresrev.2009.12.001

Meyer, N., Richter, N., Fan, Z., Siemonsmeier, G., Pivneva, T., Jordan, P., Steinhäuser, C., Semtner, M., Nolte, C., & Kettenmann, H. (2018). Oligodendrocytes in the mouse corpus callosum maintain axonal function by delivery of glucose. *Cell Reports*, 22(9), 2383–2394. https://doi.org/10.1016/j.celrep.2018.02.022

Miller, R. H., & Raff, M. C. (1984). Fibrous and protoplasmic astrocytes are biochemically and developmentally distinct. *Journal of Neuroscience*, 4(2), 585–592. https://doi.org/10.1523/JNEUROSCI.04-02-00585.1984

Miller, S. J. (2018). Astrocyte heterogeneity in the adult central nervous system. *Frontiers in Cellular Neuroscience*, 12, 1–6. https://doi.org/10.3389/fncel.2018.00401

Mongeon, R., Venkatachalam, V., & Yellen, G. (2016). Cytosolic NADH-NAD$^+$ redox visualized in brain slices by two-photon fluorescence lifetime biosensor imaging. *Antioxidants & Redox Signaling*, 25(10), 553–563. https://doi.org/10.1089/ars.2015.6593

Morland, C., Henjum, S., Iversen, E. G., Skrede, K. K., & Hassel, B. (2007). Evidence for a higher glycolytic than oxidative metabolic activity in white matter of rat brain. *Neurochemistry International*, 50(5), 703–709. https://doi.org/10.1016/j.neuint.2007.01.003

Nave, K. A. (2010a). Myelination and support of axonal integrity by glia. *Nature*, 468(7321), 244–252. https://doi.org/10.1038/nature09614

Nave, K. A. (2010b). Myelination and the trophic support of long axons. *Nature Reviews Neuroscience*, 11(4), 275–283. https://doi.org/10.1038/nrn2797

Newman, E. A. (1986). High potassium conductance in astrocyte endfeet. *Science*, 233(4762), 453–454. https://doi.org/10.1126/science.3726539

Norenberg, M. D., & Martinez-Hernandez, A. (1979). Fine structural localization of glutamine synthetase in astrocytes of rat brain. *Brain Research*, 161(2), 303–310. https://doi.org/10.1016/0006-8993(79)90071-4

Nortley, R., & Attwell, D. (2017). Control of brain energy supply by astrocytes. *Current Opinion in Neurobiology*, 47, 80–85. https://doi.org/10.1016/j.conb.2017.09.012

Oberheim, N. A., Goldman, S. A., & Nedergaard, M. (2012). Heterogeneity of astrocytic form and function. *Methods in Molecular Biology*, 814, 23–45. https://doi.org/10.1007/978-1-61779-452-0_3

Oe, Y., Baba, O., Ashida, H., Nakamura, K. C., & Hirase, H. (2016). Glycogen distribution in the microwave-fixed mouse brain reveals heterogeneous astrocytic patterns. *Glia*, 64(9), 1532–1545. https://doi.org/10.1002/glia.23020

Oheim, M., Schmidt, E., & Hirrlinger, J. (2018). Local energy on demand: Are 'spontaneous' astrocytic Ca^{2+}-microdomains the regulatory unit for astrocyte-neuron metabolic cooperation? *Brain Research Bulletin*, 136, 54–64. https://doi.org/10.1016/j.brainresbull.2017.04.011

Pantoni, L., Garcia, J. H., & Gutierrez, J. A. (1996). Cerebral white matter is highly vulnerable to ischemia. *Stroke*, 27(9), 1641–1647. https://doi.org/10.1161/01.str.27.9.1641

Parpura, V., & Zorec, R. (2010). Gliotransmission: Exocytotic release from astrocytes. *Brain Research Reviews*, 63(1–2), 83–92. https://doi.org/10.1016/j.brainresrev.2009.11.008

Pätz, C., Brachtendorf, S., & Eilers, J. (2018). The transgenic mouse line Igsf9-eGFP allows targeted stimulation of inferior olive efferents. *Journal of Neuroscience Methods*, 296, 84–92. https://doi.org/10.1016/j.jneumeth.2017.12.024

Pellerin, L., & Magistretti, P. J. (1994). Glutamate uptake into astrocytes stimulates aerobic glycolysis: A mechanism coupling neuronal activity to glucose utilization. *Proceedings of the National Academy of Sciences*, 91(22), 10625–10629. https://doi.org/10.1073/pnas.91.22.10625

Pellerin, L., & Magistretti, P. J. (2012). Sweet sixteen for ANLS. *Journal of Cerebral Blood Flow & Metabolism*, 32(7), 1152–1166. https://doi.org/10.1038/jcbfm.2011.149

Pierre, K., & Pellerin, L. (2005). Monocarboxylate transporters in the central nervous system: Distribution, regulation and function. *Journal of Neurochemistry*, 94(1), 1–14. https://doi.org/10.1111/j.1471-4159.2005.03168.x

Poolos, N. P., Mauk, M. D., & Kocsis, J. D. (1987). Activity-evoked increases in extracellular potassium modulate presynaptic excitability in the CA1 region of the hippocampus. *Journal of Neurophysiology*, 58(2), 404–416. https://doi.org/10.1152/jn.1987.58.2.404

Rash, J. E. (2010). Molecular disruptions of the panglial syncytium block potassium siphoning and axonal saltatory conduction: Pertinence to neuromyelitis optica and other demyelinating diseases of the central nervous system. *Neuroscience*, 168(4), 982–1008. https://doi.org/10.1016/j.neuroscience.2009.10.028

Regan, M. R., Huang, Y. H., Kim, Y. S., Dykes-Hoberg, M. I., Jin, L., Watkins, A. M., Bergles, D. E., & Rothstein, J. D. (2007). Variations in promoter activity reveal a differential expression and physiology of glutamate transporters by glia in the developing and mature CNS. *Journal of Neuroscience*, 27(25), 6607–6619. https://doi.org/10.1523/JNEUROSCI.0790-07.2007

Reichenbach, A., Derouiche, A., & Kirchhoff, F. (2010). Morphology and dynamics of perisynaptic glia. *Brain Research Reviews*, 63(1–2), 11–25. https://doi.org/10.1016/j.brainresrev.2010.02.003

Requardt, R. P., Hirrlinger, P. G., Wilhelm, F., Winkler, U., Besser, S., & Hirrlinger, J. (2012). Ca^{2+} signals of astrocytes are modulated by the NAD^+/NADH redox state. *Journal of Neurochemistry*, 120(6), 1014–1025. https://doi.org/10.1111/j.1471-4159.2012.07645.x

Rimmele, T. S., Castro Abrantes, H. D., Wellbourne-Wood, J., Lengacher, S., & Chatton, J.-Y. (2018). Extracellular potassium and glutamate interact to modulate mitochondria in astrocytes. *ACS Chemical Neuroscience*, 9(8), 2009–2015. https://doi.org/10.1021/acschemneuro.8b00124

Rimmele, T. S., Rocher, A. B., Wellbourne-Wood, J., & Chatton, J.-Y. (2017). Control of glutamate transport by extracellular potassium: Basis for a negative feedback on synaptic transmission. *Cerebral Cortex*, 27(6), 3272–3283. https://doi.org/10.1093/cercor/bhx078

Rose, C. R., Ziemens, D., Untiet, V., & Fahlke, C. (2018). Molecular and cellular physiology of sodium-dependent glutamate transporters. *Brain Research Bulletin*, 136, 3–16. https://doi.org/10.1016/j.brainresbull.2016.12.013

Ruminot, I., Gutiérrez, R., Peña-Münzenmayer, G., Añazco, C., Sotelo-Hitschfeld, T., Lerchundi, R., Niemeyer, M. I., Shull, G. E., & Barros, L. F. (2011). NBCe1 mediates the acute stimulation of astrocytic glycolysis by extracellular K^+. *Journal of Neuroscience*, 31(40), 14264–14271. https://doi.org/10.1523/JNEUROSCI.2310-11.2011

Ruminot, I., Schmälzle, J., Leyton, B., Barros, L. F., & Deitmer, J. W. (2017). Tight coupling of astrocyte energy metabolism to synaptic activity revealed by genetically encoded FRET nanosensors in hippocampal tissue. *Journal of Cerebral Blood Flow & Metabolism*, 39(3), 513–523. https://doi.org/10.1177/0271678X17737012

Rutter, J., Reick, M., Wu, L. C., & McKnight, S. L. (2001). Regulation of clock and NPAS2 DNA binding by the redox state of NAD cofactors. *Science*, 293(5529), 510–514. https://doi.org/10.1126/science.1060698

Saab, A. S., Tzvetavona, I. D., Trevisiol, A., Baltan, S., Dibaj, P., Kusch, K., Mobius, W., Goetze, B., Jahn, H. M., Huang, W., Steffens, H.,

Schomburg, E. D., Perez-Samartin, A., Perez-Cerda, F., Bakhtiari, D., Matute, C., Lowel, S., Griesinger, C., Hirrlinger, J., ... Nave, K. A. (2016). Oligodendroglial NMDA receptors regulate glucose import and axonal energy metabolism. *Neuron*, 91(1), 119–132. https://doi.org/10.1016/j.neuron.2016.05.016

Sagar, S. M., Sharp, F. R., & Swanson, R. A. (1987). The regional distribution of glycogen in rat brain fixed by microwave irradiation. *Brain Research*, 417(1), 172–174. https://doi.org/10.1016/0006-8993(87)90195-8

San Martín, A., Arce-Molina, R., Aburto, C., Baeza-Lehnert, F., Barros, L. F., Contreras-Baeza, Y., Pinilla, A., Ruminot, I., Rauseo, D., & Sandoval, P. Y. (2022). Visualizing physiological parameters in cells and tissues using genetically encoded indicators for metabolites. *Free Radical Biology & Medicine*, 182, 34–58. https://doi.org/10.1016/j.freeradbiomed.2022.02.012

San Martín, A., Ceballo, S., Baeza-Lehnert, F., Lerchundi, R., Valdebenito, R., Contreras-Baeza, Y., Alegría, K., & Barros, L. F. (2014). Imaging mitochondrial flux in single cells with a FRET sensor for pyruvate. *PLoS One*, 9(1), e85780. https://doi.org/10.1371/journal.pone.0085780

San Martín, A., Ceballo, S., Ruminot, I., Lerchundi, R., Frommer, W. B., & Barros, L. F. (2013). A genetically encoded FRET lactate sensor and its use to detect the Warburg effect in single cancer cells. *PLoS One*, 8(2), e57712. https://doi.org/10.1371/journal.pone.0057712

San Martín, A., Sotelo-Hitschfeld, T., Lerchundi, R., Fernandez-Moncada, I., Ceballo, S., Valdebenito, R., Baeza-Lehnert, F., Alegria, K., Contreras-Baeza, Y., Garrido-Gerter, P., Romero-Gomez, I., & Barros, L. F. (2014). Single-cell imaging tools for brain energy metabolism: A review. *Neurophotonics*, 1(1), 1–9. https://doi.org/10.1117/1.NPh.1.1.011004

Schindelin, J., Arganda-Carreras, I., Frise, E., Kaynig, V., Longair, M., Pietzsch, T., Preibisch, S., Rueden, C., Saalfeld, S., Schmid, B., Tinevez, J. Y., White, D. J., Hartenstein, V., Eliceiri, K., Tomancak, P., & Cardona, A. (2012). Fiji: An open-source platform for biological-image analysis. *Nature Methods*, 9(7), 676–682. https://doi.org/10.1038/nmeth.2019

Schitine, C., Nogaroli, L., Costa, M. R., & Hedin-Pereira, C. (2015). Astrocyte heterogeneity in the brain: From development to disease. *Frontiers in Cellular Neuroscience*, 9, 1–11. https://doi.org/10.3389/fncel.2015.00076

Shannon, C., Salter, M., & Fern, R. (2007). GFP imaging of live astrocytes: Regional differences in the effects of ischaemia upon astrocytes. *Journal of Anatomy*, 210(6), 684–692. https://doi.org/10.1111/j.1469-7580.2007.00731.x

Sickmann, H. M., Walls, A. B., Schousboe, A., Bouman, S. D., & Waagepetersen, H. S. (2009). Functional significance of brain glycogen in sustaining glutamatergic neurotransmission. *Journal of Neurochemistry*, 109(Suppl. 1), 80–86. https://doi.org/10.1111/j.1471-4159.2009.05915.x

Sofroniew, M. V., & Vinters, H. V. (2010). Astrocytes: Biology and pathology. *Acta Neuropathologica*, 119(1), 7–35. https://doi.org/10.1007/s00401-009-0619-8

Sokoloff, L., Reivich, M., Kennedy, C., Des Rosiers, M. H., Patlak, C. S., Pettigrew, K. D., Sakurada, O., & Shinohara, M. (1977). The [^{14}C]deoxyglucose method for the measurement of local cerebral glucose utilization: Theory, procedure, and normal values in the conscious and anesthetized albino rat. *Journal of Neurochemistry*, 28(5), 897–916. https://doi.org/10.1111/j.1471-4159.1977.tb10649.x

Somjen, G. G. (1988). Nervenkitt: Notes on the history of the concept of neuroglia. *Glia*, 1(1), 2–9. https://doi.org/10.1002/glia.440010103

Sotelo-Hitschfeld, T., Fernandez-Moncada, I., & Barros, L. F. (2012). Acute feedback control of astrocytic glycolysis by lactate. *Glia*, 60(4), 674–680. https://doi.org/10.1002/glia.22304

Sotelo-Hitschfeld, T., Niemeyer, M. I., Machler, P., Ruminot, I., Lerchundi, R., Wyss, M. T., Stobart, J., Fernandez-Moncada, I., Valdebenito, R., Garrido-Gerter, P., Contreras-Baeza, Y., Schneider, B. L., Aebischer, P., Lengacher, S., San Marin, A., Le

Douce, J., Bonvento, G., Magistretti, P. J., Sepulveda, F. V., ... Barros, L. F. (2015). Channel-mediated lactate release by K$^+$-stimulated astrocytes. _Journal of Neuroscience_, _35_(10), 4168–4178. https://doi.org/10.1523/JNEUROSCI.5036-14.2015

Stobart, J. L., Ferrari, K. D., Barrett, M. J. P., Stobart, M. J., Looser, Z. J., Saab, A. S., & Weber, B. (2018). Long-term in vivo calcium imaging of astrocytes reveals distinct cellular compartment responses to sensory stimulation. _Cerebral Cortex_, _28_(1), 184–198. https://doi.org/10.1093/cercor/bhw366

Swanson, R. A., Sagar, S. M., & Sharp, F. R. (1989). Regional brain glycogen stores and metabolism during complete global ischaemia. _Neurological Research_, _11_(1), 24–28. https://doi.org/10.1080/01616412.1989.11739856

Tani, H., Dulla, C. G., Farzampour, Z., Taylor-Weiner, A., Huguenard, J. R., & Reimer, R. J. (2014). A local glutamate-glutamine cycle sustains synaptic excitatory transmitter release. _Neuron_, _81_(4), 888–900. https://doi.org/10.1016/j.neuron.2013.12.026

Tekkok, S. B., Brown, A. M., Westenbroek, R., Pellerin, L., & Ransom, B. R. (2005). Transfer of glycogen-derived lactate from astrocytes to axons via specific monocarboxylate transporters supports mouse optic nerve activity. _Journal of Neuroscience Research_, _81_(5), 644–652. https://doi.org/10.1002/jnr.20573

Tekkok, S. B., & Ransom, B. R. (2004). Anoxia effects on CNS function and survival: Regional differences. _Neurochemical Research_, _29_(11), 2163–2169. https://doi.org/10.1007/s11064-004-6890-0

Trevisiol, A., Kusch, K., Steyer, A. M., Gregor, I., Nardis, C., Winkler, U., Köhler, S., Restrepo, A., Möbius, W., Werner, H. B., Nave, K.-A., & Hirrlinger, J. (2020). Structural myelin defects are associated with low axonal ATP levels but rapid recovery from energy deprivation in a mouse model of spastic paraplegia. _PLoS Biology_, _18_(11), e3000943. https://doi.org/10.1371/journal.pbio.3000943

Trevisiol, A., Saab, A. S., Winkler, U., Marx, G., Imamura, H., Möbius, W., Kusch, K., Nave, K. A., & Hirrlinger, J. (2017). Monitoring ATP dynamics in electrically active white matter tracts. _eLife_, _6_, 1–17. https://doi.org/10.7554/eLife.24241

Tyurikova, O., Shih, P.-Y., Dembitskaya, Y., Savtchenko, L. P., McHugh, T. J., Rusakov, D. A., & Semyanov, A. (2022). K$^+$ efflux through postsynaptic NMDA receptors suppresses local astrocytic glutamate uptake. _Glia_, _70_(5), 961–974. https://doi.org/10.1002/glia.24150

Waitt, A. E., Reed, L., Ransom, B. R., & Brown, A. M. (2017). Emerging roles for glycogen in the CNS. _Frontiers in Molecular Neuroscience_, _10_, 1–10. https://doi.org/10.3389/fnmol.2017.00073

Wake, H., Lee, P. R., & Fields, R. D. (2011). Control of local protein synthesis and initial events in myelination by action potentials. _Science_, _333_(6049), 1647–1651. https://doi.org/10.1126/science.1206998

Walz, W. (2000). Role of astrocytes in the clearance of excess extracellular potassium. _Neurochemistry International_, _36_(4–5), 291–300. https://doi.org/10.1016/s0197-0186(99)00137-0

Wang, D. D., & Bordey, A. (2008). The astrocyte odyssey. _Progress in Neurobiology_, _86_(4), 342–367. https://doi.org/10.1016/j.pneurobio.2008.09.015

Wender, R., Brown, A. M., Fern, R., Swanson, R. A., Farrell, K., & Ransom, B. R. (2000). Astrocytic glycogen influences axon function and survival during glucose deprivation in central white matter. _Journal of Neuroscience_, _20_(18), 6804–6810. https://doi.org/10.1523/JNEUROSCI.20-18-06804.2000

Winkler, U., & Hirrlinger, J. (2015). Crosstalk of signaling and metabolism mediated by the NAD$^+$/NADH redox state in brain cells. _Neurochemical Research_, _40_(12), 2394–2401. https://doi.org/10.1007/s11064-015-1526-0

Winkler, U., Hirrlinger, P. G., Sestu, M., Wilhelm, F., Besser, S., Zemljic-Harpf, A. E., Ross, R. S., Bornschein, G., Krugel, U., Ziegler, W. H., & Hirrlinger, J. (2013). Deletion of the cell adhesion adaptor protein

vinculin disturbs the localization of GFAP in Bergmann glial cells. _Glia_, _61_(7), 1067–1083. https://doi.org/10.1002/glia.22495

Winkler, U., Seim, P., Enzbrenner, Y., Köhler, S., Sicker, M., & Hirrlinger, J. (2017). Activity-dependent modulation of intracellular ATP in cultured cortical astrocytes. _Journal of Neuroscience Research_, _95_(11), 2172–2181. https://doi.org/10.1002/jnr.24020

Wu, O., Cloonan, L., Mocking, S. J. T., Bouts, M. J. R. J., Copen, W. A., Cougo-Pinto, P. T., Fitzpatrick, K., Kanakis, A., Schaefer, P. W., Rosand, J., Furie, K. L., & Rost, N. S. (2015). Role of acute lesion topography in initial ischemic stroke severity and long-term functional outcomes. _Stroke_, _46_(9), 2438–2444. https://doi.org/10.1161/STROKEAHA.115.009643

Xu, J., Song, D., Xue, Z., Gu, L., Hertz, L., & Peng, L. (2013). Requirement of glycogenolysis for uptake of increased extracellular K$^+$ in astrocytes: Potential implications for K$^+$ homeostasis and glycogen usage in brain. _Neurochemical Research_, _38_(3), 472–485. https://doi.org/10.1007/s11064-012-0938-3

Yamasaki, M., Yamada, K., Furuya, S., Mitoma, J., Hirabayashi, Y., & Watanabe, M. (2001). 3-Phosphoglycerate dehydrogenase, a key enzyme for L-serine biosynthesis, is preferentially expressed in the radial glia/astrocyte lineage and olfactory ensheathing glia in the mouse brain. _Journal of Neuroscience_, _21_(19), 7691–7704. https://doi.org/10.1523/JNEUROSCI.21-19-07691.2001

Yeh, T. H., Lee, D. Y., Gianino, S. M., & Gutmann, D. H. (2009). Microarray analyses reveal regional astrocyte heterogeneity with implications for neurofibromatosis type 1 (NF1)-regulated glial proliferation. _Glia_, _57_(11), 1239–1249. https://doi.org/10.1002/glia.20845

Yi, C.-X., Habegger, K. M., Chowen, J. A., Stern, J., & Tschöp, M. H. (2011). A role for astrocytes in the central control of metabolism. _Neuroendocrinology_, _93_(3), 143–149. https://doi.org/10.1159/000324888

Ying, W. (2007). NAD$^+$ and NADH in brain functions, brain diseases and brain aging. _Frontiers in Bioscience_, _12_(58), 1863–1888. https://doi.org/10.14714/CP58.261

Zhang, Y., & Barres, B. A. (2010). Astrocyte heterogeneity: An underappreciated topic in neurobiology. _Current Opinion in Neurobiology_, _20_(5), 588–594. https://doi.org/10.1016/j.conb.2010.06.005

Zippin, J. H., Chen, Y., Straub, S. G., Hess, K. C., Diaz, A., Lee, D., Tso, P., Holz, G. G., Sharp, G. W. G., Levin, L. R., & Buck, J. (2013). CO$_2$/HCO$_3{}^-$ and calcium-regulated soluble adenylyl cyclase as a physiological ATP sensor. _Journal of Biological Chemistry_, _288_(46), 33283–33291. https://doi.org/10.1074/jbc.M113.510073

Ziskin, J. L., Nishiyama, A., Rubio, M., Fukaya, M., & Bergles, D. E. (2007). Vesicular release of glutamate from unmyelinated axons in white matter. _Nature Neuroscience_, _10_(3), 321–330. https://doi.org/10.1038/nn1854

Zuend, M., Saab, A. S., Wyss, M. T., Ferrari, K. D., Hösli, L., Looser, Z. J., Stobart, J. L., Duran, J., Guinovart, J. J., Barros, L. F., & Weber, B. (2020). Arousal-induced cortical activity triggers lactate release from astrocytes. _Nature Metabolism_, _2_(2), 179–191. https://doi.org/10.1038/s42255-020-0170-4

SUPPORTING INFORMATION

Additional supporting information can be found online in the Supporting Information section at the end of this article.